liposome complexes in melanoma: expression, biologic activity, and lack of toxicity in humans, Proc. Natl. Acad. Sci. U. S. A. 90 (1993) 11307–11311.

[7] E.G. Nabel, Z. Yang, D. Muller, A.E. Chang, X. Gao, L. Huang, K.J. Cho, G.J. Nabel, Safety and toxicity of catheter gene delivery to the pulmonary vasculature in a patient with metastatic melanoma, Hum. Gene Ther. 5 (1994) 1089–1094.

[8] T. Endo, K. Inoue, S. Nojima, T. Sekiya, K. Ohki, Y. Nozawa, Electron microscopic study on the structures formed by mixtures containing synthetic glyceroglycolipids, J. Biochem. (Tokyo) 93 (1983) 1–6.

[9] T.M. Allen, C. Hansen, J. Rutledge, Liposomes with prolonged circulation times: factors affecting uptake by reticuloendothelial and other tissues, Biochim. Biophys. Acta 981 (1989) 27–35.

[10] Y. Inoh, D. Kitamoto, N. Hirashima, M. Nakanishi, Biosurfactants of MEL-A increase gene transfection mediated by cationic liposomes, Biochem. Biophys. Res. Commun. 289 (2001) 57–61.

[11] D. Kitamoto, H. Yanagishita, T. Shinbo, C. Kamisawa, T. Nakane, T. Nakahara, Surface active properties and antimicrobial activities of mannosylerythritol lipids as biosurfactants produced by *Candida antarctica*, J. Biotechnol. 29 (1993) 91–96.

[12] D. Kitamoto, G. Sangita, G. Ourisson, Y. Nakatani, Formation of giant vesicles from diacylmannosylerythritols, and their binding to concanavalin A, Chem. Commun. (2000) 861–862.

[13] Isoda, H. Shinmoto, D. Kitamoto, M. Matsumura, T. Nakahara, Differentiation of human promyelocytic leukemia cell line HL60 by microbial extracellular glycolipids, Lipids 32 (1997) 263–271.

[14] Y. Wakamatsu, X. Zhao, C. Jin, N. Day, M. Shibahara, N. Nomura, T. Nakahara, T. Murata, K.K. Yokoyama, Mannosylerythritol lipid induces characteristics of neuronal differentiation in PC12 cells through an ERK-related signal cascade, Eur. J. Biochem. 268 (2001) 374–383.

[15] Y. Inoh, D. Kitamoto, N. Hirashima, M. Nakanishi, Biosurfactant MEL-A dramatically increases gene transfection via membrane fusion, J. Control. Release 94 (2004) 423–431.

[16] Y. Hattori, Y. Maitani, Enhanced in vitro DNA transfection efficiency by novel folate-linked nanoparticles in human prostate cancer and oral cancer, J. Control. Release 97 (2004) 173–183.

[17] M. Nakanishi, New strategy in gene transfection by cationic transfection lipids with a cationic cholesterol, Curr. Med. Chem. 10 (2003) 1289–1296.

[18] I.M. Banat, R.S. Makkar, S.S. Cameotra, Potential commercial applications of microbial surfactants, Appl. Microbiol. Biotechnol. 53 (2000) 495–508.

[19] S.S. Cameotra, R.S. Makkar, Synthesis of biosurfactants in extreme conditions, Appl. Microbiol. Biotechnol. 50 (1998) 520–529.

Available online at www.sciencedirect.com
SCIENCE DIRECT
ELSEVIER
International Journal of Pharmaceutics 316 (2006) 109–116
INTERNATIONAL JOURNAL OF PHARMACEUTICS
www.elsevier.com/locate/ijpharm

Design, synthesis and gene delivery efficiency of novel oligo-arginine-linked PEG-lipids: Effect of oligo-arginine length

Masahiko Furuhata [a], Hiroko Kawakami [b], Kazunori Toma [b], Yoshiyuki Hattori [a], Yoshie Maitani [a,*]

[a] *Institute of Medicinal Chemistry, Hoshi University, Ebara 2-4-41, Shinagawa-ku, Tokyo 142-8501, Japan*
[b] *The Noguchi Institute, Kaga 1-8-1, Itabashi-ku, Tokyo 173-0003, Japan*

Received 17 September 2005; received in revised form 2 February 2006; accepted 24 February 2006
Available online 4 April 2006

Abstract

The design, synthesis, and evaluation of in vitro gene delivery efficacy of a novel series of oligo-Arg-lipid conjugates are described. 3,5-Bis(dodecyloxy)benzamide (BDB) was employed as the lipid component, and a poly(ethylene glycol) (PEG) spacer was introduced between the C-terminal of oligo-Arg and the amide group of BDB. Four derivatives with various oligo-Arg lengths (ArgN-PEG-BDB; $N=4$, 6, 8, 10: the number of arginine residues) were prepared, and the effect of oligo-Arg length on the gene transfection was investigated in HeLa cells. Transfection efficiency increased as the number of arginine residues increased. Arg10-PEG-BDB showed the highest transfection efficiency, without severe toxicity to cells. These findings well corresponded to the cellular association of the Arg-PEG-BDB/DNA complex determined by flow cytometry. Even in the presence of serum, Arg10-PEG-BDB achieved appreciable cellular association and attained high gene expression. Thus, Arg10-PEG-BDB is potentially a simple and useful gene delivery tool, because one need only to mix it with plasmid DNA and apply the complexes to the cells even in a serum-containing medium.

Keywords: Cell penetrating peptides; Oligo-arginine; Gene delivery

1. Introduction

Cationic lipid-based gene transfection constitutes one of the most promising alternatives to the use of viral vectors (Felgner et al., 1987; Song et al., 1998; Cotten et al., 1990; Kircheis et al., 1999; Brown et al., 2000). However, the low-level transfection efficiency compared with viral vectors is considered a major limitation in the application to gene therapy. The poor efficiency is supposed to arise from the endocytic route of internalization of cationic lipids complexed with DNA. Therefore, novel and more efficient synthetic vectors, hopefully with a different cell internalization mechanism, are desired.

Recently, a cellular internalization method using short peptides derived from protein-transduction domains has attracted much attention. Several cell penetrating peptides (CPPs), such as HIV-1 Tat fragments, less than 30 amino acid residues in length, have the capability of crossing a plasma membrane (Derossi et al., 1994; Vives et al., 1997; Oehlke et al., 1998; Pooga et al., 1998; Futaki et al., 2001a; Morris et al., 2001). In addition, they can deliver their associated molecules into cells. The Tat peptide has been reported to be capable of delivering β-galactosidase (120 kDa) to various organs when administered intraperitoneally to mice (Schwarze et al., 1999), and even nanoparticles (Lewin et al., 2000) and liposomes (Torchilin et al., 2001) can be delivered into cells. Although the mechanism of cell internalization is still incompletely understood, it is reported to be different from that of liposome vectors, which are internalized via an energy-independent pathway (Derossi et al., 1994; Vives et al., 1997). Oligo-arginine (Arg) conjugates were demonstrated to have characteristics similar to CPPs in cell translocation (Mitchell et al., 2000; Wender et al., 2000; Futaki et al., 2001a).

Although investigations delineating the influence of Arg length on the transfection efficiency and uptake of oligo-Args have been reported (Mitchell et al., 2000; Wender et al., 2000; Futaki et al., 2001a,b), there is no report about oligo-Arg-linked poly(ethylene glycol) (PEG) lipids alone as a gene vector. The

* Corresponding author. Tel.: +81 3 5498 5048; fax: +81 3 5498 5048.
E-mail address: yoshie@hoshi.ac.jp (Y. Maitani).

0378-5173/$ – see front matter © 2006 Elsevier B.V. All rights reserved.
doi:10.1016/j.ijpharm.2006.02.041

aim of this study was to design and synthesize simple and effective vectors for use in gene delivery. Oligo-Arg-linked PEG-lipids might have the ability to electrostatically stabilize naked DNA and mediate gene transfection through a non-endocytotic pathway.

In the present study, we synthesized oligo-Arg-lipids of quite different structure from a reported one (Futaki et al., 2001b), employing 3,5-bis (dodecyloxy)benzamide (BDB) as the lipid component, and introducing a PEG spacer between the C-terminal of oligo-Arg and the amide group of BDB (oligo-Arg-PEG-BDB). Four derivatives with various oligo-Arg lengths were prepared, and the effect of oligo-Arg length on the gene delivery efficacy was investigated in HeLa cells. We demonstrate that the arginine 10-mer exhibits the highest transfection efficiency in HeLa cells among our series of compounds.

2. Materials and methods

2.1. Materials

All amino acid derivatives and coupling reagents were obtained from Kokusan chemical Co., LTD (Tokyo, Japan). PEG 2000 was obtained from Kanto Kagaku Co., Ltd (Tokyo, Japan), and converted into its diamino derivative using a reported procedure (Slama and Rando, 1980). 9-fluorenylmethyloxycarbonyl-[Arg(2,2,4,6,7-pentamethyldihydrobenzofuran-5-sulfonyl)]$_6$-OH (Fmoc-[Arg(Pbf)]$_6$-OH) was purchased from Peptide Institute, Inc (Osaka, Japan). The Pica gene luciferase assay kit was purchased from Toyo Ink (Tokyo, Japan). Bicinchonic acid (BCA) protein assay reagent and EZ-Label Fluorescein Protein Labeling Kit were obtained from Pierce (Rockford, IL, USA). Lipofectamine™ 2000, fluorescein isothiocyanate (FITC)-transferrin and Dulbecco's modified Eagle's medium (DMEM) were purchased from Invitrogen Corp. (Carlsbad, CA, USA). FITC-Tat was purchased from AnaSpec, Inc. (San Jose, CA, USA). All other chemicals used were of reagent grade. Fetal bovine serum (FBS) was purchased from Life Technologies (Grand Island, NY, USA). In the following section, the number of moles of PEG in compounds is calculated by taking the molecular weight of the PEG fragment as 2000.

2.2. Synthesis of oligo-Arg-PEG-BDBs

3,5-Bis(dodecyloxy)benzoic acid (Balagurusamy et al., 1997) (1 g) and benzotriazol-1-yl-oxy-tris-pyrrolidino-phosphonium hexafluorophosphate (PyBOP) (0.38 g) were dissolved in *N,N*-dimethylformamide (DMF) (30 mL), and the solution was stirred at room temperature for 1 h. Diamino poly(ethylene glycol) 2000 (5 g) was added to the solution, and the reaction was carried out overnight. The resulting mixture was poured into water, and extracted with $CHCl_3$. The organic layer was washed with water, dried over $MgSO_4$, and filtered, and the organic solvent was evaporated under reduced pressure. The residue was purified by silica gel column chromatography to give **1** (Fig. 1). Fmoc-Arg(2,2,5,7,8-pentamethylchroman-6-sulfonyl (Pmc))-OH (1.07 g) and PyBOP (0.84 g) were dissolved in DMF

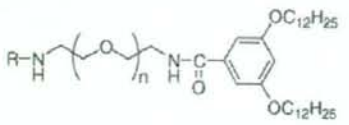

1 R = H	**9** R = Arg_4 (Arg4-PEG-BDB)
2 R = Fmoc-Arg(Pmc)	**10** R = Fmoc-[Arg(Pbf)]$_6$
3 R = Arg(Pmc)	**11** R = Arg_6 (Arg6-PEG-BDB)
4 R = Fmoc-[Arg(Pmc)]$_2$	**12** R = Fmoc-[Arg(Pbf)]$_6$[Arg(Pmc)]$_2$
5 R = [Arg(Pmc)]$_2$	**13** R = Arg_8 (Arg8-PEG-BDB)
6 R = Fmoc-[Arg(Pmc)]$_3$	**14** R = [Arg(Pmc)]$_4$
7 R = [Arg(Pmc)]$_3$	**15** R = Fmoc-[Arg(Pbf)]$_6$[Arg(Pmc)]$_4$
8 R = Fmoc-[Arg(Pmc)]$_4$	**16** R = Arg_{10} (Arg10-PEG-BDB)

Fig. 1. Chemical structures of ArgN-PEG-BDBs and their synthetic intermediates.

(20 mL), and the solution was stirred at room temperature for 1 h. **1** (2 g) was added to the solution, and the reaction was carried out overnight. The resulting mixture was poured into water, and extracted with $CHCl_3$. The organic layer was washed with water, dried over $MgSO_4$, filtered, and the organic solvent was evaporated under reduced pressure. The residue was purified by Sephadex LH-20 to give **2**. To a solution of **2** (2.45 g) in CH_2Cl_2, piperidine was added, and the solution was stirred at room temperature for 30 min. The resulting mixture was directly purified using Sephadex LH-20 to give **3**. Similarly, **4**, **5**, **6**, **7** and **8** were synthesized step by step. A solution of **8** (0.2 g) in trifluoroacetic acid (TFA)/water (9/1, 2 mL) was stirred at room temperature for 3 h, and concentrated in vacuo. The residue was dissolved in CH_2Cl_2. Piperidine was added to the solution, and the reaction carried out at room temperature for 30 min. The resulting mixture was directly purified by silica gel column chromatography to give Arg4-PEG-BDB (**9**). MALDI-TOF MS (α-CHCA) 3096.13, 3140.03, 3184.71 ([M+H]$^+$). Similar to the synthesis of **2** and **8**, **10** and Arg6-PEG-BDB (**11**), respectively, were synthesized from Fmoc-[Arg(Pbf)]$_6$-OH and **1**. MALDI-TOF MS (α-CHCA) 3584.62, 3628.17, 3672.29 ([M + H]$^+$). Similar to the synthesis of **2** and **8**, **12** and Arg8-PEG-BDB (**13**), respectively, were synthesized from Fmoc-[Arg(Pbf)]$_6$-OH and **5**. MALDI-TOF MS (α-CHCA) 3670.02, 3714.17, 3757.87 ([M+H]$^+$). Similar to the deprotection of the Fmoc group of **2** and **8** gave **14**. Similar to the synthesis of **2** and **8**, **15** and Arg10-PEG-BDB (**16**), respectively, were synthesized from Fmoc-[Arg(Pbf)]$_6$-OH and **14**. MALDI-TOF MS (α-CHCA) 4123.36, 4166.18, 4209.92 ([M + H]$^+$).

2.3. Plasmid DNA and FITC-labeled oligodeoxynucleotide

The plasmid DNA (about 6740 bp) encoding the luciferase gene under the control of the CMV promoter (pCMV-luc) was supplied by Dr. Tanaka of the Mt. Sinai School of Medicine (NY, USA). The plasmid pEGFP-C1 encoding the green fluorescent protein (GFP) under the CMV promoter was purchased from Clontech (Palo Alto, CA, USA). Protein-free preparations of pCMV-luc and pEGFP-C1 were purified following alkaline lysis using maxiprep columns (Qiagen, Hilden, Germany). The

FITC-labeled 20-mer randomized oligodeoxynucleotide (FITC-labeled ODN) was synthesized with a phosphodiester backbone (Sigma Genosys Japan, Hokkaido, Japan).

2.4. Preparation of FITC-labeled Arg10-PEG-BDB

FITC-labeled Arg10-PEG-BDB was prepared by applying an EZ-Label Fluorescein Protein Labeling Kit to Arg10-PEG-BDB.

2.5. Cell culture

Human cervical carcinoma cells (HeLa) were kindly provided by Toyobo Co., Ltd. (Osaka, Japan). HeLa cells were grown in DMEM supplemented with 10% FBS at 37 °C in a humidified 5% CO_2 atmosphere.

2.6. Gene transfection

An aqueous solution of plasmid DNA (pCMV-luc or pEGFP-C1) or FITC-labeled ODN was added to the oligo-Arg-PEG-BDB aqueous solution with gentle shaking to form oligo-Arg-PEG-BDB/DNA complexes. Each complex was left at room temperature for 10–15 min. HeLa cell cultures were prepared by plating cells in a 35-mm culture dish 24 h prior to each experiment. The cells were washed 3 times with 1 mL of serum-free DMEM. For transfection, each oligo-Arg-PEG-BDB/DNA complex (2 μg of plasmid DNA and 100 μg of oligo-Arg-PEG-BDB per well were fixed with a charge ratio (+/−) of oligo-Arg to plasmid DNA of 4.25–5.5 (Arg4-PEG-BDB-Arg10-PEG-BDB)) was diluted with serum-free DMEM to 1 mL, then gently applied to the cells. Two sets of conditions were employed: (a) after incubation for 3 h at 37 °C in serum-free DMEM, DMEM (1 mL) containing 10% FBS was added, and the cells were further incubated for 21 h, (b) incubation for 24 h at 37 °C in DMEM (2 mL) containing 10% FBS. For transfection with Lipofectamine™ 2000, 5 μL of Lipofectamine™ 2000 was used for 2 μg of the plasmid DNA to form a DNA complex in Opti-MEM according to the manufacturer's protocol. The incubation conditions were the same as stated above. The measurement of gene transfer efficiency was performed in triplicate.

2.7. Inhibition of endocytosis

Arg10-PEG-BDB (100 μg) containing 20% FITC-labeled Arg10-PEG-BDB or its complex with plasmid DNA (2 μg), FITC-transferrin and FITC-Tat were diluted with DMEM containing 10% FBS to 1 mL and then incubated with cells for 3 h at either 4 °C or 37 °C.

2.8. Luciferase assay

Luciferase expression was measured according to the instructions accompanying the luciferase assay system. Incubation was terminated by washing the plates three times with cold phosphate buffered saline (pH 7.4) (PBS). Cell lysis solution (Pica gene) was added to the cell monolayers and subjected to freezing at −80 °C and thawing at 37 °C, followed by centrifugation at 15,000 rpm for 5 s. The supernatants were frozen and stored at −80 °C until the assays. Aliquots of 20 μL of the supernatants were mixed with 100 μL of luciferase assay system (Pica gene) and counts per second (cps) were measured with a chemoluminometer (Wallac ARVO SX 1420 multilabel counter, Perkin-Elmer Life Science, Japan, Co. Ltd., Kanagawa, Japan). The protein concentration of the supernatants was determined with BCA reagent using bovine serum albumin as a standard and cps/μg protein was calculated.

2.9. Flow cytometry

At the end of the incubation, the dishes were washed two times with 1 mL of PBS, and the cells were detached with 0.05% trypsin and EDTA solution. The cells were centrifuged at 1500×*g*, and the supernatant was discarded. The cells were resuspended with PBS containing 0.1% BSA and 1 mM EDTA, and directly introduced to a FACSCalibur flow cytometer (Becton Dickinson, San Jose, CA, USA) equipped with a 488 nm argon ion laser. Data for 10,000 fluorescent events were obtained by recording forward scatter (FSC) and side scatter (SSC) with green (530/30 nm) fluorescence.

2.10. Confocal microscopy

GFP expression in HeLa cells was observed after the gene transfection with incubation for 3 h at 37 °C in serum-free DMEM. DMEM (1 mL) containing 10% FBS was added as described above. After the medium was removed, the cells were washed with PBS and fixed with 10% formaldehyde PBS at room temperature for 20 min, and washed three times with PBS. Then, the cells were coated with Aqua Poly/Mount (Poly science, Warrington, PA, USA) to prevent fading and covered with coverslips. The fixed cells were observed with a Radiance 2100 confocal laser scanning microscope (BioRad, CA, USA). GFP was imaged using the 488-nm excitation beam of an argon laser, and fluorescence emission was observed with a filter HQ515/30. The contrast level and brightness of the images were adjusted.

2.11. Particle size determination

The oligo-Arg-PEG-BDB/DNA complex and Lipofectamine™ 2000/DNA complex were formed as described in Gene Transfection. Particle size was measured by the dynamic light-scattering method (ELS-800, Otsuka Electronics Co. Ltd, Osaka, Japan) at 25 °C after diluting the Arg-PEG-BDB/DNA complex, the Lipofectamine™ 2000/DNA complex, Lipofectamine™ 2000 and Arg10-PEG-BDB to an appropriate volume with Milli-Q water.

2.12. Cytotoxicity

HeLa cells were seeded at a density of 1×10^4 cells per well in 96-well plates and maintained for 24 h before transfection in DMEM supplemented with 10% FBS. The cells were washed

with serum-free DMEM. The culture medium was replaced with serum-free DMEM (50 μL) including various concentrations of Arg10-PEG-BDB ranging from 2.5 to 1000 μM, or the DNA complex as described in Section 2.6. After incubation for 3 h at 37 °C with serum-free DMEM (50 μL), DMEM (50 μL) containing 10% FBS was added. The cells were further incubated for 21 h. The number of surviving cells was determined by a WST-8 assay (Dojindo Laboratories, Kumamoto, Japan). Cell viability was expressed as the ratio of the A_{450} of cells treated with the DNA complex to that of the control samples.

2.13. Data analysis

Significant differences in the mean values were evaluated by student's unpaired *t*-test. A *p*-value of less than 0.05 was considered significant.

3. Results

3.1. Luciferase expression of Arg-PEG-BDB/DNA complexes

We prepared four oligo-Arg-linked lipids of various lengths, Arg4-PEG-BDB, Arg6-PEG-BDB, Arg8-PEG-BDB and Arg10-PEG-BDB (Fig. 1). We evaluated the transfection efficiency of oligo-Arg-PEG-BDB by assaying luciferase activity. HeLa cells were transfected with oligo-Arg-PEG-BDB complexed with pCMV-luc. Transfection was conducted for 3 h in the absence or presence of serum, and the cells were cultured for another 21 h in the presence of serum. According to the result of a preliminary experiment, the oligo-Arg-PEG-BDB concentration appeared to be an important factor in obtaining a high transfection efficiency. All oligo-Arg-PEG-BDB derivatives exhibited luciferase activity at 40 μg/mL with a charge ratio of cation to plasmid of 2.2–1.7 (Arg4-PEG-BDB-Arg10-PEG-BDB). As the concentration of oligo-Arg-PEG-BDB increased, the level of luciferase activity also increased. However, it was observed that Arg8-PEG-BDB became cytotoxic at 200 μg/mL in the gene transfection. Therefore, the concentration of oligo-Arg-PEG-BDB should be restricted. A concentration of 100 μg/mL, corresponding to 32, 29, 27 and 25 μM for Arg4-PEG-BDB, Arg6-PEG-BDB, Arg8-PEG-BDB and Arg10-PEG-BDB, respectively, was used in the subsequent experiments.

Fig. 2(A) and (B) demonstrates that the longer oligo-Arg showed stronger luciferase activity irrespective of the serum in the medium. Arg10-PEG-BDB showed the highest level of activity among the oligo-Arg-PEG-BDB derivatives, with about 40-fold, 11-fold and 4-fold higher transfection efficiencies than Arg4-PEG-BDB, Arg6-PEG-BDB and Arg8-PEG-BDB, respectively, on 3 h-incubation in serum-free medium (Fig. 2(A)). Arg10-PEG-BDB showed about 1/5 the transfection efficiency of Lipofectamine™ 2000, a commercial gene transfection reagent, even in a serum-containing medium (Fig. 2(B)). Serum tended to decrease the gene transfection efficiency of oligo-Arg-PEG-BDB, an exception being Arg10-PEG-BDB.

3.2. Cellular uptake of Arg-PEG-BDB/DNA complexes

To confirm the ability of oligo-Arg-PEG-BDB to carry genes into cells, we prepared ODN labeled with FITC and assayed the cell internalization of the Arg8-PEG-BDB, Arg10-PEG-BDB/ODN or Lipofectamine™ 2000 complex by flow cytometry (Fig. 3). Cells were exposed for 3 h to the FITC-labeled ODN complex in the absence (Fig. 3(A)) or presence of serum (Fig. 3(B)), cultured for another 21 h in the presence of serum, and then trypsinized. A flow cytometric analysis demonstrated that cell internalization occurred in each case and in the absence of serum, Lipofectamine™ 2000 showed the strongest labeling

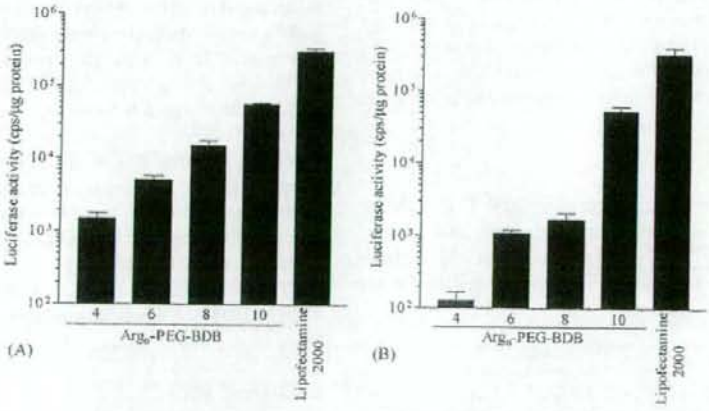

Fig. 2. In vitro luciferase activity after transfection of HeLa cells using oligo-Arg-PEG-BDB/DNA complexes. The complexes were prepared by mixing 2 μg of pCMV-luc with 100 μg of oligo-Arg-PEG-BDB or Lipofectamine™ 2000 (5 μL). The charge ratio of cation to plasmid was 4.25–5.5 (Arg4-PEG-BDB-Arg10-PEG-BDB). (A) After incubation for 3 h at 37 °C in serum-free DMEM, DMEM (1 mL) containing 10% FBS was added, and the cells were further incubated for 21 h. (B) Cells were incubated for 24 h at 37 °C in DMEM (2 mL) containing 10% FBS. Each bar represents the mean ± S.D. of three experiments.

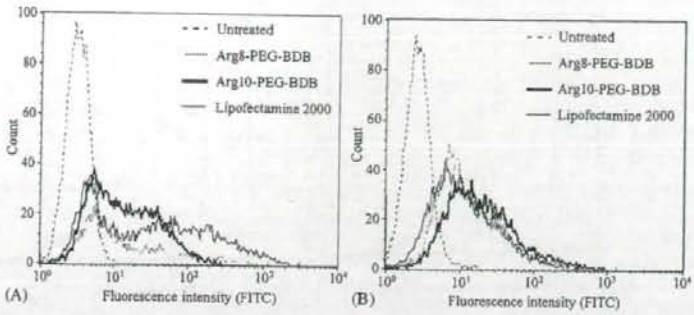

Fig. 3. Cellular uptake of the DNA complexes of Arg8-PEG-BDB and Arg10-PEG-BDB. Arg8-PEG-BDB, Arg10-PEG-BDB (100 μg) or Lipofectamine™ 2000 was mixed with 2 μg of FITC-labeled ODN. (A) The cells were incubated for 3 h in serum-free DMEM and incubated another 21 h in DMEM containing 10% FBS. (B) The cells were incubated for 24 h in DMEM (2 mL) containing 10% FBS and treated with trypsin before FACS analysis. Rough dotted line, untreated; Subtle dotted line, Arg8-PEG-BDB; Bold line, Arg10-PEG-BDB; Plain line, Lipofectamine™ 2000.

intensity among vectors. However, in the presence of serum, the intensity of the signal was greater in the cells transfected with Arg10-PEG-BDB than those with Lipofectamine™ 2000 and Arg8-PEG-BDB, indicating that Arg10-PEG-BDB could carry more DNA into the cells than Lipofectamine™ 2000 and Arg8-PEG-BDB. It suggests that the uptake efficiency of Arg10-PEG-BDB was not susceptible to the serum. These results suggest that the optimal number of oligo-Arg was 10 among the tested. Therefore, Arg10-PEG-BDB was used in subsequent experiments.

3.3. GFP gene transfection

To examine the distribution of transfection in cells, we observed the transfection efficiency of Arg10-PEG-BDB with the plasmid pEGFP-C1 using confocal microscopy. Cells were exposed for 3 h to the Arg10-PEG-BDB or Lipofectamine™ 2000/DNA complex in the absence of serum, and then cultured for another 21 h in the presence of serum. Next, the cells were fixed with 10% paraformaldehyde and visualized by confocal microscopy (Fig. 4). A slightly lower level of GFP protein was observed in the cells treated with Arg10-PEG-BDB than with Lipofectamine™ 2000, corresponding to the results of luciferase expression (Fig. 2). Similar results were obtained in a flow cytometric study for Arg10-PEG-BDB and Lipofectamine™ 2000 in serum-free incubation (Fig. 3(A)).

3.4. Effect of low temperature on the uptake

To confirm the internalization mechanism of our CPP, we prepared FITC-labeled Arg10-PEG-BDB and examined the effect of temperature on the cellular uptake of complexes. In order to avoid changes in the cell internalization character, we only incorporated FITC-labeled Arg10-PEG-BDB (20%). The endocytosis marker transferrin (Tf) and another CPP of Tat were used as control. The cells were exposed to FITC-labeled Arg10-PEG-BDB or its DNA complex, FITC-transferrin and FITC-Tat for 3 h at either 4 °C or 37 °C in the presence of serum. Then, the cells were trypsinized and analyzed by flow cytometry (Fig. 5). FITC-labeled Arg10-PEG-BDB and its DNA complex showed about an 86% lower internalization efficiency at 4 °C than at 37 °C. No significant difference in the mean fluorescence was observed between the DNA complex and FITC-labeled Arg10-PEG-BDB alone at 4 and 37 °C (Fig. 5(C)). This finding suggests that the internalization by our oligo-Arg-PEG-BDB and its DNA complexes was considerably inhibited at low temperature.

3.5. Particle size

Particle sizes of Arg10-PEG-BDB, Lipofectamine™ 2000, Arg10-PEG-BDB/DNA and Lipofectamine™ 2000/DNA were estimated using dynamic light scattering in Milli-Q water 15–60 min after the complex had formed. Particles of

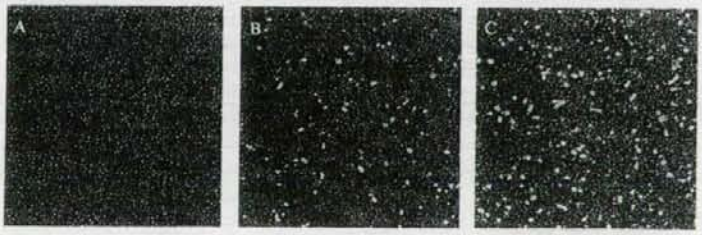

Fig. 4. Analysis of GFP expression by confocal microscopy. The DNA complexes were prepared by mixing 2 μg of pEGFP with Arg10-PEG-BDB (100 μg) or Lipofectamine™ 2000 (5 μL). The cells were incubated for 3 h in serum-free DMEM and incubated another 21 h in DMEM (1 mL) containing 10% FBS before confocal microscopy. Panel A, untreated; panel B, Arg10-PEG-BDB; panel C, Lipofectamine™ 2000. All views were recorded with the same camera acquisition parameters.

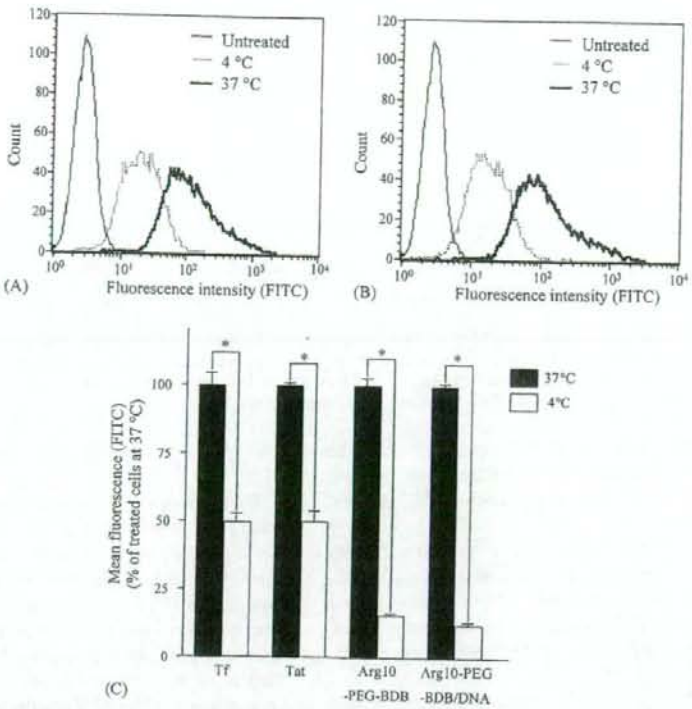

Fig. 5. Effect of temperature on the cellular uptake of FITC-labeled Arg10-PEG-BDB and its DNA complexes. (A) Arg10-PEG-BDB containing 20% FITC-labeled Arg-PEG-BDB. (B) The complex of plasmid DNA with FITC-labeled Arg10-PEG-BDB. Arg10-PEG-BDB was labeled with fluorescein isothiocyanate at the N-terminal of oligo-Arg as described under experimental procedures. The DNA complexes were prepared by mixing 2 μg of plasmid DNA with FITC-labeled Arg10-PEG-BDB (100 μg). The cells were incubated for 3 h at 4 or 37 °C in DMEM (1 mL) containing 10% FBS, and treated with trypsin before flow cytometry. (C) The mean fluorescence intensity of FITC-labeled Arg10-PEG-BDB, its DNA complexes, FITC-transferrin (Tf) (25 μg/mL) and FITC-Tat (Tat) (10 μM) compared with treated cells at 37 and 4 °C. Closed bar, 37 °C; Open bar, 4 °C. Each bar represents the mean ± S.D. of three experiments. $p < 0.05$ are marked by asterisk.

Arg10-PEG-BDB and the Arg10-PEG-BDB/DNA complex were about 300 and 1000 nm, respectively, suggesting that Arg10-PEG-BDB formed micelles. Those of Lipofectamine™ 2000 and the Lipofectamine™ 2000/DNA complex were about 400 nm and about 800 nm, respectively.

3.6. Cytotoxicity

The cytotoxicity of the vectors was assessed by the WST-8 assay using cells incubated with Arg10-PEG-BDB in serum-free medium for 3 h and in a serum-containing medium for another 21 h. The IC_{50} value was about 550 μM for Arg10-PEG-BDB (data not shown). The cytotoxicity of the Arg10-PEG-BDB/DNA complex was almost equal to that of the Lipofectamine™ 2000/DNA complex in both sets of conditions (Fig. 6).

4. Discussion

A peptide consisting of oligo-Arg has been shown to be translocated through cell membranes as efficiently as other CPPs (Mitchell et al., 2000; Wender et al., 2000; Futaki et al., 2001a). In these cases, the oligo-Arg length and the hydrophobic moiety of oligo-Arg conjugates were important factors for the uptake and transfection in cells (Futaki et al., 2001b). The aims of this study were to design and synthesize novel oligo-Arg-linked PEG-lipids, and determine the optimal length of oligo-Arg for transfection efficiency and to develop an effective gene delivery vector.

We prepared oligo-Arg-modified lipids with a PEG linker. The transfection experiment using pCMV-luc showed the ability of oligo-Arg-PEG-BDB to carry genes into cells. The transfection efficiency of the longer oligo-Arg was higher. The transfection efficiency in the absence of serum increased about four times as two arginine residues were added. The highest level of luciferase activity in cells was observed in Arg10-PEG-BDB irrespective of serum, suggesting that the optimal number of arginine residues for transfection was 10.

A limitation of the transfection assay with pCMV-luc is that it does not provide any information on the percentage of cells transfected. Therefore, we used pEGFP-C1 as another plasmid DNA. Arg10-PEG-BDB showed a similar efficiency in gene transfer to pCMV-luc, and a slightly lower fluorescence to Lipofectamine™ 2000, on confocal microscopy and flow cytometry in serum-free medium. The transfection assay with pEGFP-C1 and Arg10-PEG-BDB provided evidence that the

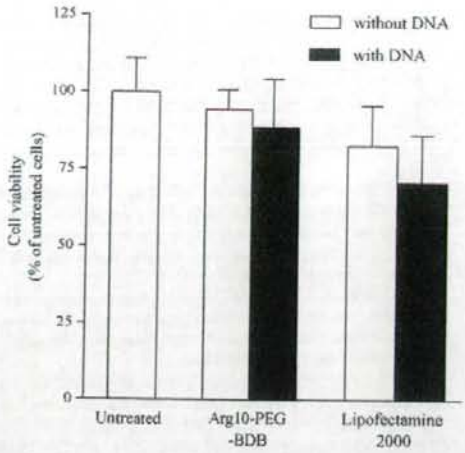

Fig. 6. Cytotoxicity of Arg10-PEG-BDB and Lipofectamine™ 2000 complexed with the plasmid DNA. The cytotoxicity on transfection was evaluated using the WST-8 assay. HeLa cells were seeded at a density of 1×10^4 cells per well in 96-well plates and maintained for 24 h before the gene transfection in DMEM containing 10% FBS. The culture medium was replaced with serum-free DMEM (50 μL) containing DNA (2 μg) complexed with Arg10-PEG-BDB (100 μg) or with Lipofectamine™ 2000 (5 μL). After incubation for 3 h at 37 °C in DMEM without FBS, DMEM (50 μL) containing 10% FBS was added. The cells were further incubated for another 21 h. Open bars, cell viability in the absence of plasmid DNA; Closed bars, cell viability in the presence of plasmid DNA. Each bar represents the mean ± S.D. of three experiments.

observed transfection efficiency resulted from low overall levels of gene insertion in many cells, not from a low overall percentage of cells transfected with a few cells receiving large numbers of the reporter gene.

We also showed that both Arg8-PEG-BDB and Arg10-PEG-BDB were able to carry plasmid DNA inside the cells by flow cytometry. To removing the surface bound Arg-PEG-BDB/DNA complexes, we washed the cells with PBS and treated them with trypsin (Richard et al., 2003). In the presence of serum, Arg10-PEG-BDB was able to deliver more DNA into the cells than Lipofectamine™ 2000 and Arg8-PEG-BDB, but this finding did not reflect in transfection efficiency. It was suggested that the process of cellular uptake and/or transfection might be different between Arg10-PEG-BDB and Lipofectamine™ 2000. No severe cytotoxicity was observed during 24 h incubation at 25 μM (100 μg/mL) of Arg10-PEG-BDB (Fig. 6). Notably, even in the presence of serum, the Arg10-PEG-BDB/DNA complex achieved appreciable cellular association to attain a high level of gene expression.

Mitchell et al. reported that 15 arginine residues were internalized significantly more effectively than 20 arginine residues (Mitchell et al., 2000). Wender et al. reported that nine arginine residues, the maximum number used in their experiment, were superior to shorter oligomers in terms of cellular uptake as determined by flow cytometry (Wender et al., 2000). They also demonstrated that the presence of at least six arginine residues is important for cellular uptake (Wender et al., 2000). Using oligomers composed of 4–16 arginine residues, Futaki et al. demonstrated that there was an optimal number of arginine residues (Arg8) for cellular internalization by microscopic observation (Futaki et al., 2001a). They also reported that stearylation of Arg8 at the N-terminal (stearyl-Arg8) improved the transfection efficiency compared with Arg8 alone, giving the highest transfection efficiency from stearyl-Arg4 to stearyl-Arg16 at a charge ratio of cation to DNA of 2:1 (Futaki et al., 2001b). In our case, Arg10-PEG-BDB showed a higher transfection efficiency and cellular uptake than Arg8-PEG-BDB.

Therefore, effect of the length of oligo-Arg on transfection efficiency has to be taken into consideration. In transfection experiments with the oligo-Arg-PEG-BDB/DNA complex, the arginine residues may be partly used for translocation through the plasma membrane and partly for the formation of complex with plasmid DNA. The longer oligo-Arg would be needed for the intracellular delivery of oligo-Arg-PEG-BDB/DNA than the uptake of oligo-Arg-PEG-BDB alone. In this respect, oligo-Arg-PEG-BDB with more than ten arginine residues would be more effective for transfection if no cytotoxicity is observed. Cytotoxicity may be influenced by incubation with or without serum and/or cell type. The cellular uptake and transfection efficiency of oligo-Arg-PEG-BDB/DNA complexes were proportional to the chain length of oligo-Arg. This finding suggests that the limiting factor of gene transfection was the uptake of complex to the plasma membrane, and not the release of DNA from the endosome compartment to the cell cytoplasm or the penetration of DNA into the nucleus.

It is interesting that two quite different designs of oligo-Arg-lipids, Arg10-PEG-BDB (25 μM) (Fig. 2) and stearyl-Arg8 (30 μM) (Futaki et al., 2001b), showed comparable transfection efficiencies to Lipofectamine™ 2000. The presence of a PEG linker and the lipid structure does not seem to affect the length of oligo-Arg suitable for the transfection and uptake. The transfection efficiency is likely to be influenced more by the length of oligo-Arg than by overall structural features such as the anchor lipids, linker groups, and direction of oligo-Arg relative to the lipid portion, etc.

The cellular translocation by CPP was initially proposed to be an energy-independent process. Most papers report no difference in uptake between 37 and 4 °C (Vives et al., 1997; Futaki et al., 2001a). However, more recent papers suggest that the majority of the translocation occurs via an energy-dependent pathway and that the translocation of CPP is reduced by endocytosis inhibitors (Fischer et al., 2002; Vives, 2003; Drin et al., 2003). To investigate the internalization mechanism of our system, we constructed FITC-labeled Arg10-PEG-BDB and its DNA complex, and examined the temperature-dependence of their internalization using flow cytometry. Therefore, the internalization mechanism of our system may have less of a contribution from energy-independent processes. FITC-labeled Arg10-PEG-BDB alone showed a similar internalization efficiency to the FITC-labeled Arg10-PEG-BDB/DNA complex at 37 °C for 3 h, suggesting that Arg10-PEG-BDB and Arg10-PEG-BDB/DNA follow a similar pathway. These findings conflict with the report that the quantitative uptake of free CPP or CPP coupled to cargo can differ (Fischer et al., 2004), but corresponds to the report that the cellular entry of both stearyl-Arg8 and the stearyl-Arg8/DNA

complex occurs mainly through endocytosis (Khalil et al., 2004).

Given the particle size of Arg10-PEG-BDB, aggregates such as micelles would be formed since PEG-lipid conjugates were reported to form micelles (Lukyanov et al., 2002). One explanation for the transfection efficiency of Arg10-PEG-BDB could be that Arg10-PEG-BDB aggregates and behaves similarly to polycationic micelles (Itaka et al., 2003).

5. Conclusions

In summary, we synthesized oligo-Arg containing lipids with a PEG spacer as novel gene vectors, and found that their transfection efficiency increased as the number of arginine residues increased. Among them, Arg10-PEG-BDB showed the highest transfection efficiency in HeLa cells. Arg10-PEG-BDB and its DNA complex may be internalized via energy-dependent processes.

Acknowledgements

This project was supported in part by a grant from the Promotion and Mutual Aid Corporation for Private Schools of Japan and by a Grant-in-Aid for Scientific Research from the Ministry of Education, Culture, Sports, Science, and Technology of Japan.

References

Balagurusamy, V.S.K., Ungar, G., Percec, V., Johansson, G., 1997. Rational design of the first spherical supramolecular dendrimers self-organized in a novel thermotropic cubic liquid-crystalline phase and the determination of their shape by X-ray analysis. J. Am. Chem. Soc. 119, 1539–1555.

Brown, M.D., Schatzlein, A., Brownlie, A., Jack, V., Wang, W., Tetley, L., Gray, A.I., Uchegbu, I.F., 2000. Preliminary characterization of novel amino acid based polymeric vesicles as gene and drug delivery agents. Bioconjug. Chem. 11, 880–891.

Cotten, M., Langle-Rouault, F., Kirlappos, H., Wagner, E., Mechtler, K., Zenke, M., Beug, H., Birnstiel, M.L., 1990. Transferrin–polycation-mediated introduction of DNA into human leukemic cells: stimulation by agents that affect the survival of transfected DNA or modulate transferrin receptor levels. Proc. Natl. Acad. Sci. U.S.A. 87, 4033–4037.

Derossi, D., Joliot, A.H., Chassaing, G., Prochiantz, A., 1994. The third helix of the antennapedia homeodomain translocates through biological membranes. J. Biol. Chem. 269, 10444–10450.

Drin, G., Cottin, S., Blanc, E., Rees, A.R., Temsamani, J., 2003. Studies on the internalization mechanism of cationic cell-penetrating peptides. J. Biol. Chem. 278, 31192–31201.

Felgner, P.L., Gadek, T.R., Holm, M., Roman, R., Chan, H.W., Wenz, M., Northrop, J.P., Ringold, G.M., Danielsen, M., 1987. Lipofection: a highly efficient, lipid-mediated DNA-transfection procedure. Proc. Natl. Acad. Sci. U.S.A. 84, 7413–7417.

Fischer, R., Waizenegger, T., Kohler, K., Brock, R., 2002. A quantitative validation of fluorophore-labelled cell-permeable peptide conjugates: fluorophore and cargo dependence of import. Biochim. Biophys. Acta 1564, 365–374.

Fischer, R., Kohler, K., Fotin-Mleczek, M., Brock, R., 2004. A stepwise dissection of the intracellular fate of cationic cell-penetrating peptides. J. Biol. Chem. 279, 12625–12635.

Futaki, S., Suzuki, T., Ohashi, W., Yagami, T., Tanaka, S., Ueda, K., Sugiura, Y., 2001a. Arginine-rich peptides. An abundant source of membrane-permeable peptides having potential as carriers for intracellular protein delivery. J. Biol. Chem. 276, 5836–5840.

Futaki, S., Ohashi, W., Suzuki, T., Niwa, M., Tanaka, S., Ueda, K., Harashima, H., Sugiura, Y., 2001b. Stearylated arginine-rich peptides: a new class of transfection systems. Bioconjug. Chem. 12, 1005–1011.

Itaka, K., Yamauchi, K., Harada, A., Nakamura, K., Kawaguchi, H., Kataoka, K., 2003. Polyion complex micelles from plasmid DNA and poly(ethylene glycol)-poly(L-lysine) block copolymer as serum-tolerable polyplex system: physicochemical properties of micelles relevant to gene transfection efficiency. Biomaterials 24, 4495–4506.

Khalil, I.A., Futaki, S., Niwa, M., Baba, Y., Kaji, N., Kamiya, H., Harashima, H., 2004. Mechanism of improved gene transfer by the N-terminal stearylation of octaarginine: enhanced cellular association by hydrophobic core formation. Gene Ther. 11, 636–644.

Kircheis, R., Schuller, S., Brunner, S., Ogris, M., Heider, K.H., Zauner, W., Wagner, E., 1999. Polycation-based DNA complexes for tumor-targeted gene delivery in vivo. J. Gene Med. 1, 111–120.

Lewin, M., Carlesso, N., Tung, C.H., Tang, X.W., Cory, D., Scadden, D.T., Weissleder, R., 2000. Tat peptide-derivatized magnetic nanoparticles allow in vivo tracking and recovery of progenitor cells. Nat. Biotechnol. 18, 410–414.

Lukyanov, A.N., Gao, Z., Mazzola, L., Torchilin, V.P., 2002. Polyethylene glycol-diacyllipid micelles demonstrate increased acculumation in subcutaneous tumors in mice. Pharm. Res. 19, 1424–1429.

Mitchell, D.J., Kim, D.T., Steinman, L., Fathman, C.G., Rothbard, J.B., 2000. Polyarginine enters cells more efficiently than other polycationic homopolymers. J. Pept. Res. 56, 318–325.

Morris, M.C., Depollier, J., Mery, J., Heitz, F., Divita, G., 2001. A peptide carrier for the delivery of biologically active proteins into mammalian cells. Nat. Biotechnol. 19, 1173–1176.

Oehlke, J., Scheller, A., Wiesner, B., Krause, E., Beyermann, M., Klauschenz, E., Melzig, M., Bienert, M., 1998. Cellular uptake of an alpha-helical amphipathic model peptide with the potential to deliver polar compounds into the cell interior non-endocytically. Biochim. Biophys. Acta 1414, 127–139.

Pooga, M., Hallbrink, M., Zorko, M., Langel, U., 1998. Cell penetration by transportan. FASEB J. 12, 67–77.

Richard, J.P., Melikov, K., Vives, E., Ramos, C., Verbeure, B., Gait, M.J., Chernomordik, L.V., Lebleu, B., 2003. Cell-penetrating peptides. A reevaluation of the mechanism of cellular uptake. J. Biol. Chem. 278, 585–590.

Schwarze, S.R., Ho, A., Vocero-Akbani, A., Dowdy, S.F., 1999. In vivo protein transduction: delivery of a biologically active protein into the mouse. Science 285, 1569–1572.

Slama, J.S., Rando, R.R., 1980. Lectin-mediated aggregation of liposomes containing glycolipids with variable hydrophilic spacer arms. Biochemistry 19, 4595–4600.

Song, Y.K., Liu, F., Liu, D., 1998. Enhanced gene expression in mouse lung by prolonging the retention time of intravenously injected plasmid DNA. Gene Ther. 5, 1531–1537.

Torchilin, V.P., Rammohan, R., Weissig, V., Levchenko, T.S., 2001. TAT peptide on the surface of liposomes affords their efficient intracellular delivery even at low temperature and in the presence of metabolic inhibitors. Proc. Natl. Acad. Sci. U.S.A. 98, 8786–8791.

Vives, E., 2003. Cellular uptake of the Tat peptide: an endocytosis mechanism following ionic interactions. J. Mol. Recognit. 16, 265–271.

Vives, E., Brodin, P., Lebleu, B., 1997. A truncated HIV-1 Tat protein basic domain rapidly translocates through the plasma membrane and accumulates in the cell nucleus. J. Biol. Chem. 272, 16010–16017.

Wender, P.A., Mitchell, D.J., Pattabiraman, K., Pelkey, E.T., Steinman, L., Rothbard, J.B., 2000. The design, synthesis, and evaluation of molecules that enable or enhance cellular uptake: peptoid molecular transporters. Proc. Natl. Acad. Sci. U.S.A. 97, 13003–13008.

Novel SN-38–Incorporating Polymeric Micelles, NK012, Eradicate Vascular Endothelial Growth Factor–Secreting Bulky Tumors

Fumiaki Koizumi,[1] Masayuki Kitagawa,[2] Takahito Negishi,[1] Takeshi Onda,[2] Shin-ichi Matsumoto,[2] Tetsuya Hamaguchi,[3] and Yasuhiro Matsumura[1]

[1]Investigative Treatment Division, Research Center for Innovative Oncology, National Cancer Center Hospital East, Kashiwa, Chiba, Japan; [2]Pharmaceutical Research Laboratories, Research and Development Group, Nippon Kayaku Co., Ltd, Kita-ku, Tokyo, Japan; and [3]Department of Medicine, National Cancer Center Hospital, Tyuo-ku, Tokyo, Japan

Abstract

7-Ethyl-10-hydroxy-camptothecin (SN-38), a biological active metabolite of irinotecan hydrochloride (CPT-11), has potent antitumor activity but has not been used clinically because it is a water-insoluble drug. For delivery by i.v. injection, we have successfully developed NK012, a SN-38-releasing nanodevice. The purpose of this study is to investigate the pharmacologic character of NK012 as an anticancer agent, especially in a vascular endothelial growth factor (VEGF)–secreting tumor model. The particle size of NK012 was ~20 nm with a narrow size distribution. NK012 exhibited a much higher cytotoxic effect against lung and colon cancer cell lines as compared with CPT-11. NK012 showed significantly potent antitumor activity against a human colorectal cancer HT-29 xenograft as compared with CPT-11. Enhanced and prolonged distribution of free SN-38 in the tumor was observed after the injection of NK012. NK012 also had significant antitumor activity against bulky SBC-3/Neo (1,533.1 ± 1,204.7 mm^3) and SBC-3/VEGF tumors (1,620.7 ± 834.0 mm^3) compared with CPT-11. Furthermore, NK012 eradicated bulky SBC-3/VEGF tumors in all mice but did not eradicate SBC-3/Neo tumors. In the drug distribution analysis, an increased accumulation of SN-38 in SBC-3/VEGF tumors was observed as compared with that in SBC-3/Neo tumors. NK012 markedly enhanced the antitumor activity of SN-38, especially in highly VEGF-secreting tumors, and could be a promising SN-38-based formulation. (Cancer Res 2006; 66(20): 10048-56)

Introduction

The antitumor plant alkaloid camptothecin (CPT) is a broad-spectrum anticancer agent that targets DNA topoisomerase I. Although CPT has shown promising antitumor activity *in vitro* and *in vivo* (1, 2), it has not been clinically used because of its low therapeutic efficacy and severe toxicity (3, 4). Among CPT analogues, irinotecan hydrochloride (CPT-11) has recently been shown to be active against colorectal, lung, and ovarian cancer (5–9). CPT-11 itself is a prodrug and is converted to 7-ethyl-10-hydroxy-CPT (SN-38), a biologically active metabolite of CPT-11, by carboxylesterases. SN-38 exhibits up to 1,000-fold more potent cytotoxic activity against various cancer cells *in vitro* than CPT-11 (10). Although CPT-11 is converted to SN-38 in the liver and tumor, the metabolic conversion rate is <10% of the original volume of CPT-11 (11, 12). In addition, the conversion of CPT-11 to SN-38 depends on the genetic interindividual variability of carboxylesterase activity (13). Thus, direct use of SN-38 might be of great advantage and attractive for cancer treatment. For the clinical use of SN-38, however, it is essential to develop a soluble form of water-insoluble SN-38. The progress of the manufacturing technology of "micellar nanoparticles" may make it possible to use SN-38 for *in vivo* experiments and further clinical use.

Passive targeting of drug delivery system is based on the pathophysiologic characteristics that are observed in many solid tumors: hypervascularity, irregular vascular architecture, potential for secretion of vascular permeability factors, and the absence of effective lymphatic drainage that prevents efficient clearance of macromolecules. These characteristics, unique to solid tumors, are believed to be the basis of the enhanced permeability and retention effect (14–17). Supramolecular structures, such as liposomes and polymeric micelles, are expected to increase the accumulation of drugs in tumor tissue through these pathophysiologic features. Polymeric micelle–based anticancer drugs have been developed in recent years (18–20), and some of them have been under evaluation for clinical trials (21–23). This carrier system can incorporate various kinds of drugs into the inner core by chemical conjugation or physical entrapment with relatively high stability, and the size can be controlled within the range of 20 to 100 nm in diameter. This range of diameters is too large to pass through normal vessel walls; therefore, the drug can be expected to reduce side effects due to a decrease in volume of distribution.

Angiogenesis is essential for the growth and metastasis of solid tumors (24). The clinical importance of angiogenesis in human tumors was shown by several reports indicating a positive relationship between the blood vessel density in the tumor mass and poor prognosis for survival in patients with various types of cancers (25–28). Furthermore, Natsume et al. (29) reported that the antitumor activities of anticancer agents, including *cis*-diammine-dichloroplatinum, vincristine, and docetaxel, were less active against vascular endothelial growth factor (VEGF)–secreting cells, SBC-3/VEGF, *in vivo* as compared with its mock transfectant (SBC-3/Neo), although the high vascularity should have been favorable for the drug delivery.

VEGF is also well known as a potent vascular permeability factor (30). The ability of supramolecular structures to accumulate in target tissue is based on the enhanced tumor angiogenesis and tumor vascular permeability that occur in solid tumors. Therefore, we hypothesized that a polymeric micelle–based drug carrier would increase its accumulation and deliver enhanced therapeutic efficacy in tumors that secrete higher levels of VEGF. In the present study, we present the superiority of NK012 over CPT-11 in a tumor model,

Requests for reprints: Yasuhiro Matsumura, Investigative Treatment Division, Research Center for Innovative Oncology, National Cancer Center Hospital East, 6-5-1 Kashiwanoha, Kashiwa, Chiba 277-8577, Japan. Phone: 81-4-7134-6857; Fax: 81-4-7134-6857; E-mail: yhmatsum@east.ncc.go.jp.

doi:10.1158/0008-5472.CAN-06-1605

especially in a VEGF-secreting tumor, and we illustrate the outstanding advantage of polymeric micelle–based drug carriers.

Materials and Methods

Drugs and Cells

SN-38 was synthesized by Nippon Kayaku Co., Ltd. (Tokyo, Japan). CPT-11 was purchased from Yakult Honsha Co., Ltd. (Tokyo, Japan). Human colon cancer cell lines WiDR, SW480, Lovo, and HT-29 and human non–small-cell lung cancer cell line A431 were purchased from American Type Culture Collection (Rockville, MD). Human small-cell lung cancer cell line SBC-3 and human non–small-cell lung cancer cell line PC-14 were kindly provided by Dr. I. Kimura (Okayama University, Okayama, Japan) and Dr. Y. Hayata (Tokyo Medical University, Tokyo, Japan), respectively. SBC-3 and PC-14 were maintained in RPMI 1640 supplemented with 10% fetal bovine serum (Cell Culture Technologies, Gaggenau-Hoerden, Germany), penicillin, streptomycin, and amphotericin B (100 units/mL, 100 μg/mL, and 25 μg/mL, respectively; Sigma, St. Louis, MO) in a humidified atmosphere of 5% CO_2 at 37°C. Other cell lines were maintained in DMEM (Nikken Bio Med. Lab., Kyoto, Japan) supplemented with 10% fetal bovine serum. SBC-3/Neo and SBC-3/VEGF were generated from SBC-3 cells that were transfected with BMG-Neo and BMG-Neo-VEGF as previously reported (29). The full-length sequence of human VEGF expressing 206 amino acids (31) was selected. SBC-3/VEGF cells express ~ 100 times more soluble VEGF than SBC-3/Neo and SBC-3 cells in the supernatant of cultured cells as shown by ELISA (29).

Preparation of an SN-38–Conjugated Poly(Ethylene Glycol)-Poly(Glutamic Acid) Block Copolymer for NK012 Construction

Poly(ethylene glycol)-poly(glutamic acid) block copolymer [PEG-PGlu(SN-38)] was synthesized as follows: A poly(ethylene glycol)-poly(glutamic acid) block copolymer [PEG-PGlu] was prepared according to the previously reported technique (32, 33). SN-38 was covalently introduced into the PGlu segment by the condensation reaction between the carboxylic acid on PGlu and the phenol on SN-38 with 1,3-diisopropylcarbodiimide and *N,N*-dimethylaminopyridine at 26°C. Consequently, the PGlu segment obtained sufficient hydrophobicity. Accordingly, NK012 was constructed with self-assembling PEG-PGlu(SN-38) amphiphilic block copolymers in an aqueous milieu.

Determination of the Size Distribution of NK012 and Drug Release Behavior of SN-38 from NK012

The size distribution of NK012 was measured with the dynamic light scattering method at 25°C using a Particle Sizer NICOMP 380ZLS (Particle Sizing Systems, Santa Barbara, CA). The release behavior of SN-38 from NK012 was investigated *in vitro* at 20°C or 37°C in PBS (pH 7.3) or 5% glucose solution (pH 4.6). The concentration was 0.1 mg/mL. The amount of SN-38 released from NK012 was estimated by UV measurement at 265 nm.

In vitro Growth Inhibition Assay

The growth inhibitory effects of NK012, SN-38, and CPT-11 were examined with a 3-(4,5-dimethylthiazol-2-yl)-2,5-diphenyltetrazolium bromide (MTT) assay. One hundred eighty microliters of an exponentially growing cell suspension (6×10^3/mL-12×10^3/mL) were seeded into a 96-well microtiter plate, and 20 μL of various concentrations of each drug were added. After incubation for 72 hours at 37°C, 20 μL of MTT solution (5 mg/mL in PBS) were added to each well and the plates were incubated for an additional 4 hours at 37°C. After centrifuging the plates at 200 × *g* for 5 minutes, the medium was aspirated from each well, and 180 μL of DMSO were added to each well to dissolve the formazan. The growth inhibitory effect of each drug was assessed spectrophotometrically (SpectraMax 190, Molecular Devices Corp., Sunnyvale, CA).

In vivo Growth Inhibition Assay

The animal experimental protocols were approved by the Committee for Ethics of Animal Experimentation and the experiments were conducted in accordance with the Guidelines for Animal Experiments in the National Cancer Center or Nippon Kayaku.

Experiment 1. Female BALB/c nude mice, 7 weeks old, were purchased from CLEA Japan (Tokyo, Japan). Human colorectal cancer HT-29 cells were grown as s.c. tumor in the flank of the mice. The tumors were excised from the mice and fragments were inoculated s.c. in the mouse flank. When the tumor volume reached 70 to 170 mm^3, mice were randomly divided into test groups consisting of six mice per group (day 0). Drugs were administered on days 0, 4, and 8 by i.v. injection into the tail vein. NK012 was given at doses of 30 (maximum tolerated dose), 15, and 7.5 mg/kg/d. The reference drug, CPT-11, was given at the maximum tolerated dose, 66.7 mg/kg/d, in the optimal schedule reported (34). The length (a) and width (b) of the tumor mass were measured twice a week, and the tumor volume (TV) was calculated as follows: $TV = (a \times b^2) / 2$. Relative tumor volumes at day n were calculated according to the following formula: $RTV = TV_n / TV_0$, where TV_n is the tumor volume at day n, and TV_0 is the tumor volume at day 0. Differences in relative tumor sizes between the treatment groups at day 21 were analyzed with an unpaired t test.

Experiment 2. As a hypervascular tumor model, we used SBC-3/VEGF cells. SBC-3/Neo or SBC-3/VEGF cells (10^7) were s.c. injected into the back of mice. NK012 or CPT-11 was administered when the mean tumor volumes ($n = 4$) reached a massive size of 1,500 mm^3, which gave tumors almost 1.5 cm in length. It took ~ 65 days for SBC-3/Neo and 20 days for SBC-3/VEGF to reach the tumor volume of 1,500 mm^3 from the day of inoculation. NK012 at a dose of 10 or 20 mg/kg/d and CPT-11 at a dose of 15 or 30 mg/kg/d were administered i.v. on days 0, 4, and 8. Differences in tumor sizes between the treatment groups and control group at day 14 were analyzed with an unpaired t test.

Histologic and Immunohistochemical Analysis

Histologic sections were taken from SBC-3/Neo and SBC-3/VEGF tumor tissues when the volumes reached 1,500 mm^3. After extirpation, tissues were fixed with 3.9% formalin in PBS (pH 7.4), and the subsequent preparations and H&E staining were done by Tokyo Histopathologic Laboratory Co., Ltd. (Tokyo, Japan). For detection of tumor blood vessels, polyclonal anti–von Willebrand factor antibody (Dako, Glostrup, Denmark) was used.

Assay for SN-38 and CPT-11 in Plasma and Tissues

Female BALB/c nude mice bearing HT-29 (as mentioned in experiment 1; $n = 3$) were used for the analysis of the biodistribution of NK012 and CPT-11. NK012 (30 mg/kg) or CPT-11 (66.7 mg/kg) was administered i.v. to the mice. Under anesthesia, blood and tumor samples were taken at 5 minutes, 1, 6, 24, 48, 72, and 168 hours after administration of NK012 and at 5 minutes, 1, 3, 6, and 24 hours after administration of CPT-11. The blood samples were collected in microtubes and immediately centrifuged at 1,600 × *g* for 15 minutes. The plasma and tumor samples were stored at −80°C until analysis.

For the biodistribution study in hypervascular tumors (experiment 2), female BALB/c nude mice ($n = 3$) bearing 1,500-mm^3 massive SBC-3/Neo and SBC-3/VEGF tumors were used. NK012 (20 mg/kg) and CPT-11 (30 mg/kg) were administered on day 0. The mice were sacrificed at 1, 6, 24, and 72 hours (day 3) after administration. The tumor, liver, spleen, upper small intestine, lung, and blood were taken and stored at −80°C until analysis.

Preparation of the free SN-38 (polymer-unbound SN-38) and CPT-11. Tumor samples were homogenized on ice using a Digital homogenizer (Iuchi, Osaka, Japan) and suspended in the mixture of 100 mmol/L glycine-HCl buffer (pH 3)/methanol (1:1, v/v) at a concentration of 5% w/w. The concentrations of free SN-38 and CPT-11 in the plasma and tumor from aliquots of the homogenates (100 μL) and plasma (50 μL) were determined by high-performance liquid chromatography. For free SN-38 (polymer-unbound SN-38) and CPT-11, proteins were precipitated with an ice-cold mixture of methanol/H_2O/$HClO_4$ (50:45:5, v/v/v) containing CPT as an internal standard. The sample was vortexed for 10 seconds, filtered through a MultiScreen Solvinert (Millipore Corp., Bedford, MA), and analyzed.

Preparation of the polymer-bound SN-38 (SN-38 remaining bound to PEG-PGlu). To permit complete release of SN-38 from the conjugate, 20 μL of plasma and 100 μL of tissue samples were diluted with 20 μL of methanol (50%, v/v) and 20 μL of NaOH (0.3 mol/L for plasma and 0.7 mol/L for tissue). The samples were incubated for 15 minutes at 25°C. After incubation, 20 μL of HCl (0.3 mol/L for plasma and 0.7 mol/L for tissue) and 60 μL of internal standard solution were added to the samples, and then the hydrolysis was filtered through a MultiScreen Solvinert. The filtrate was applied to the high-performance liquid chromatography system.

High-performance liquid chromatography. Reversed-phase high-performance liquid chromatography was done at 35°C on a Mightysil RP-18 GP column 150 × 4.6 mm (Kanto Chemical Co., Inc., Tokyo, Japan). The samples were injected into an Alliance Waters 2795 high-performance liquid chromatography system (Waters, Milford, MA) equipped with a Waters 2475 multi λ fluorescence detector. The detector was set at 365 and 430 nm (excitation and emission, respectively) for CPT-11 and CPT, and at 365 and 540 nm for SN-38. A reversed-phase column was used at 35°C. The mobile phase was a mixture of 100 mmol/L ammonium acetate (pH 4.2) and methanol [11:9 (v/v) for SN-38 in plasma and tumor, 3:2 (v/v) for CPT-11 in plasma, and 63:37 (v/v) for CPT-11 in tumor]. The flow rate was 1.0 mL/min. Peak data were recorded with a chromatography management system (Empower, Waters). Polymer-bound SN-38 was determined by subtraction of polymer-unbound SN-38 from the total SN-38 of the hydrolysate.

Pharmacokinetic and Statistical Analyses

The concentrations of SN-38 and CPT-11 in plasma and tissue were fitted to a pharmacokinetic model by the nonlinear least-square method using WinNonlin Professional software (version 4.1; Pharsight Corp., Palo Alto, CA). We used a noncompartmental analysis. The pharmacokinetic variables were calculated using the following equations (AUC_{last} was calculated by the trapezoidal rule to the last measurable data point):

$$AUC_{inf} = \int_0^{\infty} C(t)dt$$

$$T_{1/2\lambda}(\text{terminal half} - \text{life}) = 0.693/\lambda z$$

(λz is first-order rate constant associated with the terminal portion of the curve)

$$CL_{tot} = \text{Dose}/AUC_{inf}$$

$$V_{ss} = MRT \times CL_{tot}\,(MRT, \text{mean residence time})$$

Data were expressed as mean ± SD. Data were analyzed with the Student's t test when the groups showed equal variances (F test) or with Welch's test when they showed unequal variances (F test). $P < 0.05$ was regarded as statistically significant. All statistical tests were two sided.

Results

Preparation and characterization of NK012. NK012 is an SN-38-loaded polymeric micelle constructed in an aqueous milieu by the self-assembly of an amphiphilic block copolymers, PEG-PGlu(SN-38). The molecular weight of PEG-PGlu(SN-38) was determined to be ~19,000 (PEG segment, 12,000; SN-38-conjugated PGlu segment, 7,000). NK012 was obtained as a freeze-dried formulation and contained ca. 20% (w/w) of SN-38 (Fig. 1*A*). The mean particle size of NK012 is 20 nm in diameter with a relatively narrow range (Fig. 1*B*). The releasing rates of SN-38 from NK012 in PBS at 37°C were 57% and 74% at 24 and 48 hours, respectively, and those in 5% glucose solution at 37°C were 1% and 3% at 24 and 48 hours, respectively (Fig. 1*C*). SN-38 is loaded by chemical bonding to the block copolymer. The bonding is phenyl ester bond, which is stable under acidic condition and labile under mild alkaline condition. These results indicate that NK012 can release SN-38 under neutral condition even without the presence of a hydrolytic enzyme and is stable in 5% glucose solution. It is suggested that NK012 is stable before administration and starts to release SN-38, the active component, under physiologic conditions after administration.

Cellular sensitivity of non-small-cell lung cancer and colon cancer cells to SN-38, NK012, and CPT-11. The IC_{50} values of NK012 for the cell lines ranged from 0.009 μmol/L (SBC-3 cells) to 0.16 μmol/L (WiDR cells). The growth inhibitory effects of NK012 are 43- to 340-fold more potent than those of CPT-11, whereas the IC_{50} values of NK012 were 2.3- to 5.8-fold higher than those of SN-38. NK012 exhibited a higher cytotoxic effect against each cell line as compared with CPT-11 (43- to 340-fold sensitivity). On the other hand, the IC_{50} values of NK012 were a little higher than those of SN-38, similar to the cytotoxic feature also reported in a previous study about micellar drugs (ref. 23; Table 1).

Antitumor activity and pharmacokinetic analysis of NK012 and CPT-11 using HT-29–bearing nude mice (experiment 1). Potent activity was observed in mice treated with NK012 at doses of 15 and 30 mg/kg (Fig. 2*A*), although neither CPT-11 at a dose of 66.7 mg/kg/d nor NK012 at a dose of 7.5 mg/kg/d exerted any significant antitumor activity *in vivo*. Comparison of the relative tumor volume at day 21 revealed significant differences between 15 mg/kg/d NK012 and 66.7 mg/kg/d CPT-11 and between 30 mg/kg/d NK012 and 66.7 mg/kg/d CPT-11 ($P < 0.05$). Although treatment-related body weight loss was observed in mice treated with each drug, body weight recovered by day 21 (Fig. 2*B*). These results clearly show the significant *in vivo* activity of NK012 against HT-29.

After injection of CPT-11, the concentrations of CPT-11 and SN-38 for plasma declined rapidly with time in a log-linear fashion. On the other hand, NK012 (polymer-bound SN-38) exhibited slower clearance (Fig. 3*A*). The clearance of NK012 in the HT-29 tumor was significantly slower and the concentration of free SN-38 was maintained at >30 ng/g even at 168 hours after injection (Fig. 3*B*). The pharmacokinetic variables of each drug in the plasma and tumor are depicted in Table 2.

Tumor-to-plasma concentration ratios (Kp) of polymer-bound and free SN-38 increased during the observation period. The highest value of Kp was achieved at 168 hours after administration, 108 for polymer-bound and 11.0 for free SN-38 (Table 3). These results indicate that NK012 can remain in the tumor tissue for a longer period and release free SN-38.

Antitumor activity and the distribution of NK012 and CPT-11 in SBC-3/Neo or SBC-3/VEGF tumors (experiment 2). To determine whether the potent antitumor effect of NK012 is enhanced in the tumors with high vascularity, we used VEGF-secreting cells SBC-3/VEGF. There was no significant difference in the *in vitro* cytotoxic activity of each drug between SBC-3/Neo and SBC-3/VEGF (Fig. 4*A*). SBC-3/VEGF tumors are reddish by gross evaluation as compared with SBC-3/Neo tumors (Fig. 4*B*). Histologic and immunohistochemical (von Willebrand factor) examination revealed that prominent leakage of erythrocytes and high vascularity were observed in SBC-3/VEGF tumor xenografts. On the other hand, SBC-3/Neo tumors have less tumor vasculatures and more interstitial space as compared with SBC-3/VEGF tumors

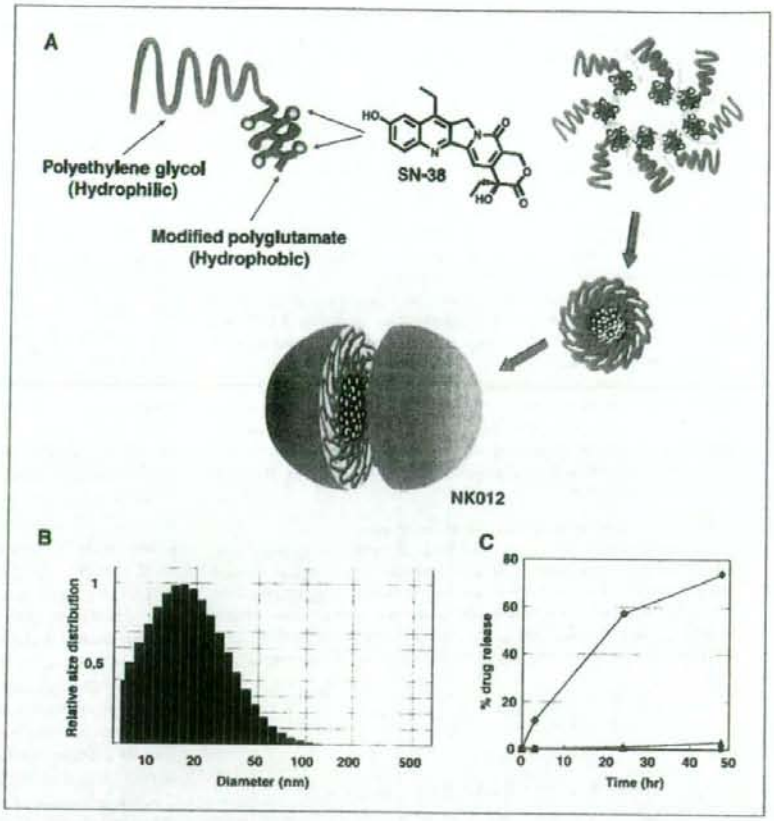

Figure 1. Preparation and characterization of NK012. *A*, schematic structure of NK012. A polymeric micelle carrier of NK012 consists of a block copolymer of PEG (molecular weight of ~ 12,000) and partially modified polyglutamate (~ 20 units). PEG (hydrophilic) is believed to be the outer shell and SN-38 was incorporated into the inner core of the micelle. *B*, size distribution of NK012 measured with the dynamic light scattering method. The *Y* axis shows relative particle size distribution. *C*, release of free SN-38 from the micelles in PBS [pH 7.3, 37°C (♦)] or 5% glucose solution [pH 4.6, 20°C (■), 37°C (▲)].

(Fig. 4*B*). Deviating from the ordinary experimental tumor model, tumors were allowed to grow until they became massive in size, ~ 1.5 cm (Fig. 4*C*), and then the treatment was initiated. NK012 at doses of 15 and 30 mg/kg showed potent antitumor activity against bulky SBC-3/Neo tumors (1,533.1 ± 1,204.7 mm^3) as compared with CPT-11 (Fig. 4*C*). Striking antitumor activity was observed in mice treated with NK012 (Fig. 4*C*) when we compared the antitumor activity of NK012 with that of CPT-11 using SBC-3/VEGF cells. SBC-3/VEGF bulky masses (1,620.7 ± 834.0 mm^3) disappeared in all mice, although relapse 3 months after treatment was noted in one mouse treated with NK012 20 mg/kg. On the other hand, SBC-3/VEGF were not eradicated and rapidly regrew after a partial response in mice treated with CPT-11. Approximately 10% body weight loss was observed in mice treated with 20 mg/kg NK012, but no significant difference was observed in comparison with mice treated with 30 mg/kg CPT-11.

We then examined the distribution of free SN-38 in the SBC-3/Neo and SBC-3/VEGF masses after administration of NK012 and CPT-11. In the case of CPT-11 administration, the concentrations at 1 and 6 hours after the administration were <100 ng/g both in the SBC-3/Neo and SBC-3/VEGF tumors and were almost negligible at 24 hours in both tumors (Fig. 5*A*). There was no significant difference in the concentration between the SBC-3/Neo and SBC-3/VEGF tumors. On the other hand, in the case of NK012 administration, free SN-38 was detectable in the tumors even at 72 hours after the administration. The concentrations of free SN-38 were higher in the SBC-3/VEGF tumors than those in the SBC-3/Neo tumors at any time point during the period of observation (significant at 1, 6, and 24 hours; $P < 0.05$; Fig. 5*A*).

Tissue distribution of SN-38 after administration of NK012 and CPT-11. We examined the concentration-time profile of free SN-38 in various tissues after i.v. administration of NK012 and

Table 1. *In vitro* growth inhibitory activity of SN-38, NK012, and CPT-11 in human lung and colorectal cancer cells (MTT assay)

Cell line	IC_{50} (μmol/L)		
	SN-38	NK012	CPT-11
WiDR	0.046 ± 0.008	0.16 ± 0.014	20.4 ± 1.6
SW480	0.025 ± 0.003	0.11 ± 0.028	31.9 ± 1.3
Lovo	0.0067 ± 0.0012	0.026 ± 0.003	7.24 ± 1.04
HT-29	0.016 ± 0.003	0.068 ± 0.007	23.1 ± 2.63
PC-14	0.044 ± 0.025	0.14 ± 0.021	5.96 ± 0.90
SBC-3	0.0016 ± 0.001	0.0093 ± 0.005	0.72 ± 0.22
A431	0.0081 ± 0.002	0.019 ± 0.007	5.6 ± 1.5

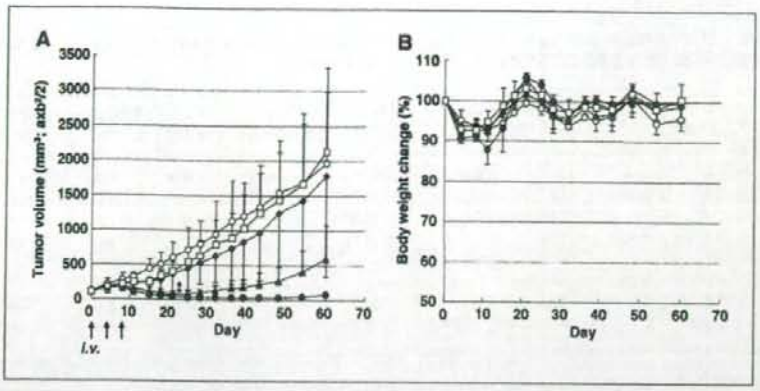

Figure 2. The effect of NK012 and CPT-11 against an HT-29 tumor xenograft. *A*, HT-29 tumor was inoculated s.c. into the flank of mice as described in Materials and Methods. CPT-11 at a dose of 66.7 mg/kg/d (□), NK012 at a dose of 7.5 mg/kg/d (♦), NK012 at a dose of 15 mg/kg/d (▲), or NK012 at a dose of 30 mg/kg/d (●) was administered i.v. on days 0, 4, and 8 (○, no treatment). Tumor volume in mice treated with CPT-11 or NK012. *Points*, mean; *bars*, SD. *, $P < 0.05$. *B*, treatment-related body weight loss occurred in mice treated with CPT-11 and NK012. *Points*, mean; *bars*, SD.

CPT-11. All organs measured exhibited the highest concentration of SN-38 at 1 hour after administration in mice given CPT-11 (Fig. 5*B*). On the other hand, mice given NK012 exhibited prolonged distribution in the liver and spleen (Fig. 5*B*). In a similar manner to other micellar drugs (19, 23), NK012 showed relatively higher accumulation in organs of the reticuloendothelial system. In the lung, kidney, and small intestine, the highest concentration of free SN-38 was achieved at 1 hour after injection of NK012 and the concentration was almost negligible at 24 hours. Although relatively high at 1 hour after administration of NK012 and CPT-11, the concentrations of free SN-38 in the small intestine rapidly decreased. Interestingly, there was no significant difference in the kinetic character of free SN-38 in the small intestine between mice treated with NK012 and CPT-11.

Discussion

The drug-incorporating polymeric micelle has characteristic pharmacokinetic features. These structures are too large to pass through normal vessel walls and evade renal excretion. The outer shell of the drug with PEG diminishes nonspecific capture by the reticuloendothelial system. Therefore, the drug can be expected to achieve a long half-life, which permits a large amount of the drug-incorporating micelles to reach the tumor site through the enhanced permeability and retention effect. The pharmacokinetic study revealed that the plasma AUC of polymer-bound SN-38 after administration of NK012 at a dose of 30 mg/kg to the HT-29-bearing mice was ~200-fold higher than that of CPT-11 at a dose of 66.7 mg/kg. A 14-fold higher AUC of the free SN-38 was achieved in mice given NK012 compared with mice given CPT-11. Prolonged circulation of NK012 in the blood might increase the accumulation of NK012 in a tumor tissue due to the enhanced permeability and retention effect. In fact, the tumor concentration of free SN-38 at 24 hours after administration of NK012 reached 90.4 ng/g and high concentrations were maintained up to 168 hours (53.1 ng/g for 48 hours, 42.6 ng/g for 72 hours, and 35.8 ng/g for 168 hours). This range of concentrations can exert sufficient antitumor activity against tumor cells. On the other hand, the concentration of CPT-11 was only 4.5 ng/g at 24 hours. These results indicate that the enhancement of tumor distribution closely contributes to the potent antitumor activity of NK012 *in vivo*.

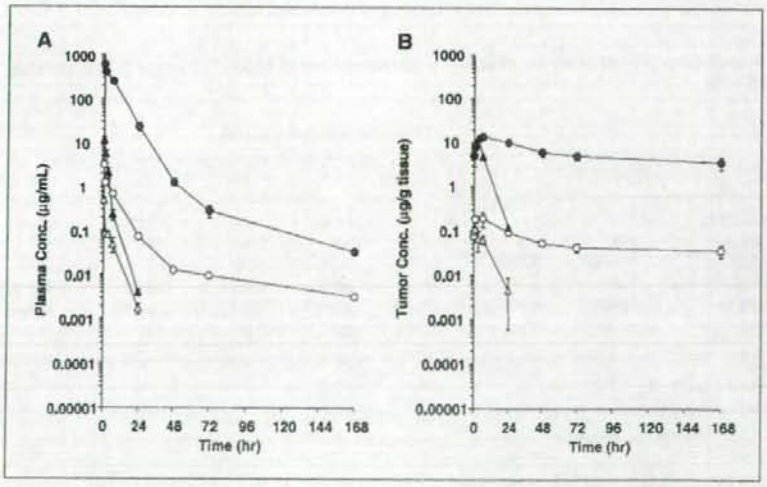

Figure 3. Plasma and tumor concentrations of respective analytes after an i.v. administration of CPT-11 (66.7 mg/kg) or NK012 (30 mg/kg) to HT-29-bearing nude mice. *A*, plasma. *B*, tumor. ●, polymer-bound SN-38; ○, free SN-38 (polymer-unbound SN-38); △, SN-38 converted from CPT-11; ▲, CPT-11.

Table 2. Pharmacokinetic variables of analytes in plasma and tumor after an i.v. administration of NK012 or CPT-11 to nude mice bearing human colon cancer HT-29 cells (NK012, 30 mg/kg; CPT-11, 66.7 mg/kg)

	Test article		C_{max} (μg/mL)	T_{max} (h)	$T_{1/2z}$ (h)	AUC_{last} (μg h/mL)	AUC_{inf} (μg h/mL)	CL_{tot} (mL/h/kg)	V_{ss} (mL/kg)	MRT_{last} (h)	$MRT_{inf.}$ (h)
Plasma	NK012	P-b SN-38*	—†	—	31.4	5,000	5,010	5.99	40.4	6.68	6.74
		P-u SN-38‡	3.10	0.0833	61.7	15.5	15.8	—	—	10.8	153
	CPT-11	CPT-11	—	—	3.08	22.1	22.2	3,010	5,420	1.78	1.80
		SN-38	0.488	0.0833	3.76	1.10	1.11	—	—	3.82	4.04
Tumor	NK012	P-b SN-38	13.8	6	—	1,010	—	—	—	62.8	—
		P-u SN-38	0.188	6	—	10.2	—	—	—	58.1	—
	CPT-11	CPT-11	12.6	3	3.36	99.7	100	—	—	4.41	4.55
		SN-38	0.108	1	4.75	1.07	1.10	—	—	5.20	5.92

NOTE: Three female nude mice were used for the analysis of biodistribution of SN-38 and CPT-11 in plasma and tissues. Data were expressed as means.
*Polymer-bound SN-38; SN-38 remaining bound to PEG-PGlu.
†Not determined.
‡Polymer-unbound SN-38; free SN-38 from PEG-PGlu.

Several preclinical studies on cytotoxic agent–incorporating polymeric micelles show their advantage as anticancer agents *in vivo* as compared with drugs of small molecular size (19, 22, 23). Because the advantage of passive targeting has been explained by the enhanced permeability and retention theory, it is essential to elucidate the correlation between the effectiveness of micellar drugs and tumor hypervascularity and hyperpermeability. We hypothesized that a polymeric micelle–based drug carrier could increase its accumulation in the tumor site and could thus enhance the therapeutic efficacy in tumors with high vascularity. To ascertain the hypothesis, we used SBC-3/VEGF. We adopted a bulky tumor model for our *in vivo* experiment to clarify the difference in activity against SBC-3/Neo and SBC-3/VEGF tumors. Histologic examination of SBC-3/VEGF showed hypervascularity and prominent leakage of erythrocytes. On the other hand, SBC-3/Neo showed hypovascularity. Our *in vivo* experiment showed that NK012 obviously enhanced its antitumor activity in SBC-3/VEGF-inplanted mice and eradicated bulky masses. It was thought that the sensitivity of cells to NK012 might not change *in vivo* because the *in vitro* sensitivity of NK012 was almost equivalent between SBC-3/Neo and SBC-3/VEGF cells. When we compared the distribution of NK012 (free SN-38) in the tumor sites, significantly enhanced accumulation was observed in the SBC-3/VEGF tumors. This strongly suggested that the drug distribution throughout the tumor site was enhanced by the hypervascularity and hyperpermeability induced by VEGF, and, subsequently, higher antitumor activity was achieved. High vascular density and enhanced vascular permeability might also be favorable for drug delivery of low molecular weight drugs. However, the SN-38 concentration was not significantly high in SBC-3/VEGF tumors after the administration of CPT-11, and tumors exhibited rapid regrowth after the treatment. We assume that such conventional low molecular size anticancer agents almost disappear from the bloodstream without being subjected to the enhanced permeability and retention effect before they can reach the target organs (solid tumor). The fact of correlation between the blood vessel density in

Table 3. Tumor-to-plasma concentration ratio (Kp) of analytes after an i.v. administration of NK012 (30 mg/kg) to nude mice bearing human colon cancer HT-29 cells

Test article	Analyte		Time after administration (h)						
			0.0833	1	6	24	48	72	168
NK012	P-b SN-38*	Plasma (μg/mL)	612	410	254	23.3	1.25	0.278	0.0333
		Tumor (μg/g)	4.99	8.00	13.8	9.95	5.90	5.03	3.58
		Kp† (mL/g)	0.00815	0.0195	0.0543	0.427	4.72	18.1	108
	P-u SN-38‡	Plasma (μg/mL)	3.10	1.24	0.673	0.0717	0.0127	0.00925	0.00325
		Tumor (μg/g)	0.0763	0.187	0.188	0.0904	0.0531	0.0426	0.0358
		Kp (mL/g)	0.0246	0.151	0.279	1.26	4.18	4.61	11.0

NOTE: Data were expressed as means of three mice.
*Polymer-bound SN-38; SN-38 remaining bound to PEG-PGlu.
†Kp values were calculated on the mean concentrations of three mice.
‡Polymer-unbound SN-38; free SN-38 from PEG-PGlu.

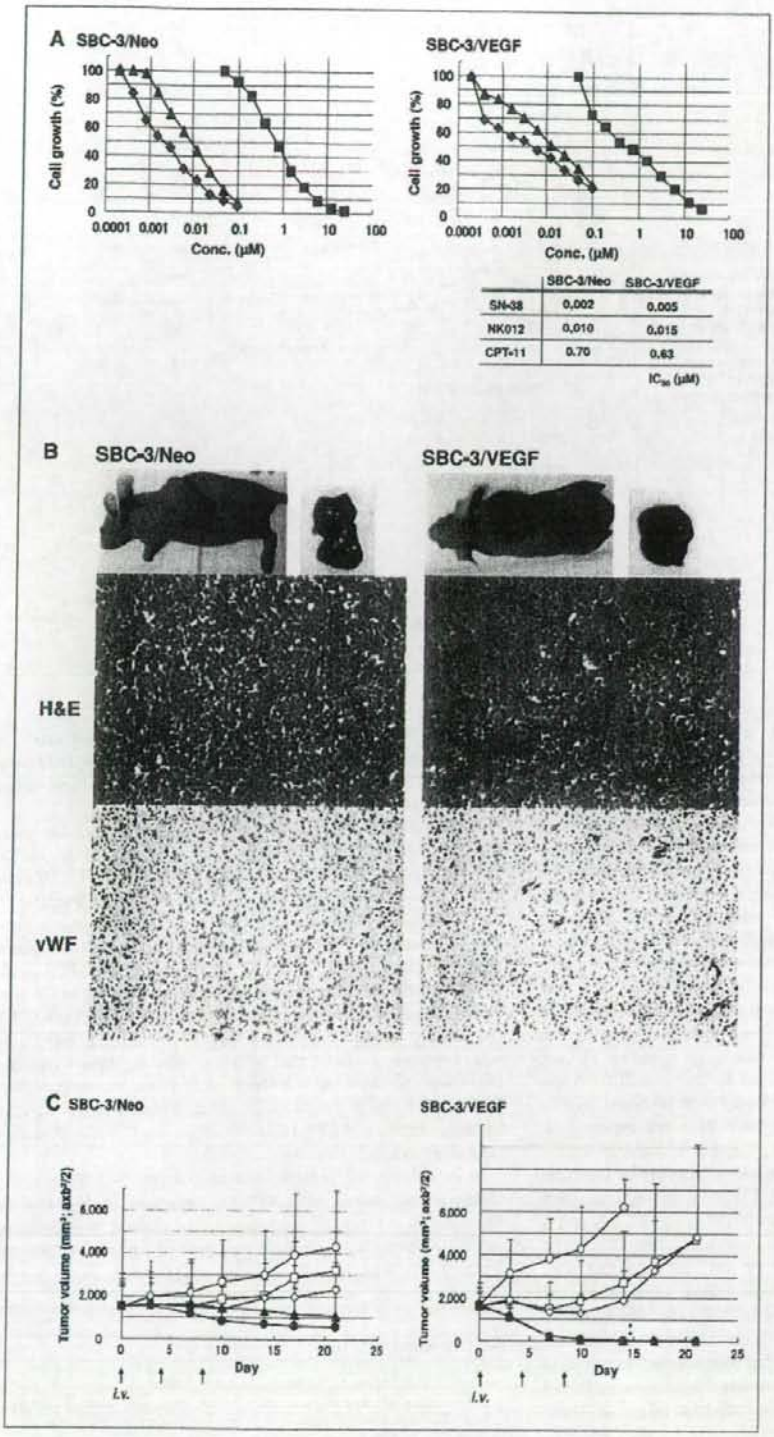

Figure 4. Growth inhibitory effect of NK012, SN-38, and CPT-11 on SBC-3/Neo and SBC-3/VEGF cells. *A*, in *in vitro* experiment, the cells were exposed to the indicated concentrations of each drug for 72 hours. The growth inhibition curves and IC_{50} values for NK012 (▲), SN-38 (◆), and CPT-11 (■) are shown. *B*, representative photographs of massive tumors developed from SBC-3/Neo and SBC-3/VEGF at the time just before treatment initiation. Histologic (H&E, ×20) and immunohistochemical (von Willebrand factor, ×20) examinations for each tumor are shown. *C*, i.v. administration of NK012 or CPT-11 was started when the mean tumor volumes of groups reached a massive size of 1,500 mm^3. The mice were divided into test groups (○, control; □, CPT-11 15 mg/kg/d; ◇, CPT-11 30 mg/kg/d; ▲, NK012 10 mg/kg/d; ●, NK012 20 mg/kg/d). NK012 or CPT-11 was administered i.v. on days 0, 4, and 8. Each group consisted of four mice. *, $P < 0.05$.

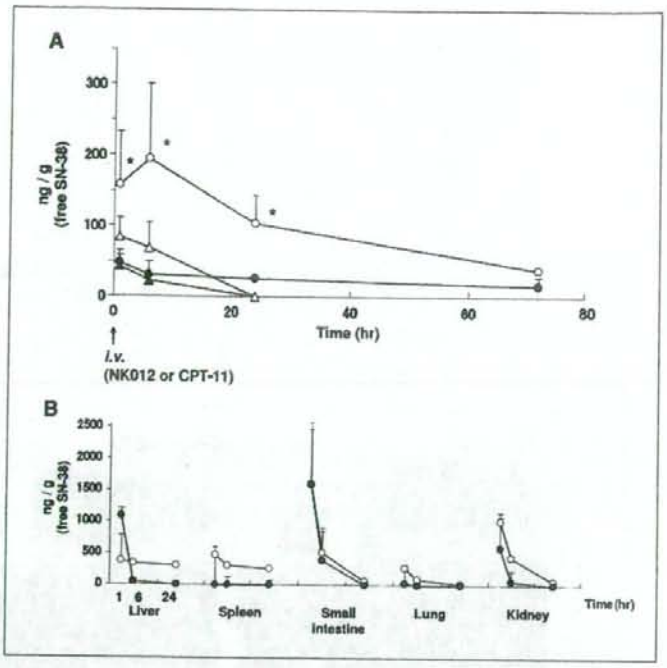

Figure 5. Tissue and tumor distribution of free SN-38 after administration of NK012 and CPT-11. *A*, time profile of free SN-38 concentration in SBC-3/Neo (●, NK012 20 mg/kg/d; ▲, CPT-11 30 mg/kg/d) and SBC-3/VEGF (○,NK012 20 mg/kg/d; △, CPT-11 30 mg/kg/d). NK012 on days 0 and 4 (96 hours) or CPT-11 on day 0 was administered. *, $P < 0.05$. *B*, tissue distribution of free SN-38 after single injection of NK012 at 30 mg/kg (○) and CPT-11 at 40 mg/kg (●).

the tumor mass and poor prognosis for survival in people with various types of cancers (25–28) supports the idea that low molecular weight drugs are not so effective in the treatment of solid tumors, which are rich in blood vessels.

Jain (35) reported that the convective passage of large drug molecules into the core of solid tumors could be impeded by abnormally high interstitial pressures in solid tumors. However, he also considered that low molecular weight anticancer agents might be harmful to normal organs because they can leak out of normal blood vessels freely; he finally concluded that one useful strategy for evading the barriers to drug dispersion would be to inject patients with drug carriers, such as liposome, filled with low molecular weight drugs. NK012 has the potential to allow the effective sustained release of SN-38 inside a tumor following the accumulation of NK012 into tumor tissue. As a matter of fact, substantial amount of SN-38 is expected to be released from the polymeric micelle. Consequently, released SN-38 becomes distributed throughout the tumor tissue and internalizes into cancer cells to kill them.

In recent years, the novel liposome-based formulation of SN-38 (LE-SN38) has been developed (36). LE-SN38 shows promising antitumor activity against various cancer cell lines (37, 38) and a clinical trial to assess its efficacy is now under way (39). The release of SN-38 from LE-SN38 is very slow as compared with NK012, ~1.9% of the drug being released from LE-SN38 in PBS buffer over 120 hours (36). The size of LE-N38 ranges from 150 to 200 nm. On the other hand, the particle size of NK012 is ~20 nm. Interestingly, Unezaki et al. (40) reported that fluorescence-labeled PEG liposomes were densely located outside the tumor vessels and stayed around the vessel walls for 2 days after i.v. injection. These data suggest that the PEG liposome is too large to move freely in the tumor interstitium and too stable to be released easily. The difference in size distribution and the character of the drug release between NK012 and LE-SN38 might influence their clinical effectiveness in the treatment of solid tumors.

One of the major toxicities associated with CPT-11 administration is severe diarrhea. Although the mechanism of the diarrhea has not yet been elucidated, one possible explanation is structural and functional injuries to the gastrointestinal tract owing to the mitotic inhibitory activity of SN-38 and CPT-11. It was reported that the number of episodes of diarrhea had a better correlation with the plasma AUC of SN-38 than with CPT-11 (41). In the present study, no difference in SN-38 accumulations in the small intestine was seen when equimolar NK012 (20 mg/kg) and CPT-11 (30 mg/kg) were administered. We also reported, using a rat mammary tumor model, that NK012 showed significant antitumor effect with diminishing incidence of diarrhea as compared with CPT-11 (42). These results suggest that diarrhea, one of the dose-limiting toxicities of CPT-11, is not augmented by the administration of NK012.

In conclusion, the present data suggest that NK012 possesses a treatment advantage over CPT-11, especially in hypervascular tumors such as renal cell carcinomas, medulloblastomas, and hepatocellular carcinomas. We have now started a phase I clinical trial for NK012 in patients with advanced solid tumors.

Acknowledgments

Received 5/3/2006; revised 7/20/2006; accepted 8/21/2006.

The costs of publication of this article were defrayed in part by the payment of page charges. This article must therefore be hereby marked *advertisement* in accordance with 18 U.S.C. Section 1734 solely to indicate this fact.

References

1. Li LH, Fraser TJ, Olin EJ, Bhuyan BK. Action of camptothecin on mammalian cells in culture. Cancer Res 1972;32:2643–50.
2. Gallo RC, Whang-Peng J, Adamson RH. Studies on the antitumor activity, mechanism of action, and cell cycle effects of camptothecin. Natl Cancer Inst 1971; 46:789–95.
3. Gottlieb JA, Guarino AM, Call JB, Oliverio VT, Block JB. Preliminary pharmacologic and clinical evaluation of camptothecin sodium (NSC-100880). Cancer Chemother Rep 1970;54:461–70.
4. Muggia FM, Creaven PJ, Hansen HH, Cohen MH, Selawry OS. Phase I clinical trial of weekly and daily treatment with camptothecin (NSC-100880): correlation with preclinical studies. Cancer Chemother Rep 1972;56: 515–21.
5. Cunningham D, Pyrhonen S, James RD, et al. Randomised trial of irinotecan plus supportive care versus supportive care alone after fluorouracil failure for patients with metastatic colorectal cancer. Lancet 1998; 352:1413–8.
6. Saltz LB, Cox JV, Blanke C, et al. Irinotecan plus fluorouracil and leucovorin for metastatic colorectal cancer. Irinotecan Study Group. N Engl J Med 2000;343: 905–14.
7. Noda K, Nishiwaki Y, Kawahara M, et al. Irinotecan plus cisplatin compared with etoposide plus cisplatin for extensive small-cell lung cancer. N Engl J Med 2002; 346:85–91.
8. Negoro S, Masuda N, Takada Y, et al. CPT-11 Lung Cancer Study Group West. Randomised phase III trial of irinotecan combined with cisplatin for advanced non-small-cell lung cancer. Br J Cancer 2003; 88:335–41.
9. Bodurka DC, Levenback C, Wolf JK, et al. Phase II trial of irinotecan in patients with metastatic epithelial ovarian cancer or peritoneal cancer. J Clin Oncol 2003; 21:291–7.
10. Takimoto CH, Arbuck SG. Topoisomerase I targeting agents: the camptothecins. In: Chabner BA, Lango DL, editors. Cancer chemotherapy and biotherapy: principal and practice. 3rd ed. Philadelphia (PA): Lippincott Williams & Wilkins; 2001. p. 579–646.
11. Slatter JG, Schaaf LJ, Sams JP, et al. Pharmacokinetics, metabolism, and excretion of irinotecan (CPT-11) following I.V. infusion of [(14)C]CPT-11 in cancer patients. Drug Metab Dispos 2000;28:423–33.
12. Rothenberg ML, Kuhn JG, Burris HA III, et al. Phase I and pharmacokinetic trial of weekly CPT-11. J Clin Oncol 1993;11:2194–204.
13. Guichard S, Terret C, Hennebelle I, et al. CPT-11 converting carboxylesterase and topoisomerase activities in tumour and normal colon and liver tissues. Br J Cancer 1999;80:364–70.
14. Matsumura Y, Maeda H. A new concept for macromolecular therapeutics in cancer chemotherapy: mechanism of tumoritropic accumulation of proteins and the antitumor agent smancs. Cancer Res 1986;46: 6387–92.
15. Dvorak HF, Nagy JA, Dvorak JT, Dvorak AM. Identification and characterization of the blood vessels of solid tumors that are leaky to circulating macromolecules. Am J Pathol 1988;133:95–109.
16. Maeda H, Matsumura Y. Tumoritropic and lymphotropic principles of macromolecular drugs. Crit Rev Ther Drug Carrier Syst 1989;6:193–210.
17. Matsumura Y, Maruo K, Kimura M, Yamamoto T, Konno T, Maeda H. Kinin-generating cascade in advanced cancer patients and *in vitro* study. Jpn J Cancer Res 1991;82:732–41.
18. Yokoyama M, Miyauchi M, Yamada N, et al. Characterization and anticancer activity of the micelle-forming polymeric anticancer drug Adriamycin-conjugated poly(ethylene glycol)-poly(aspartic acid) block copolymer. Cancer Res 1990;50:1693–700.
19. Yokoyama M, Okano T, Sakurai Y, Ekimoto H, Shibazaki C, Kataoka K. Toxicity and antitumor activity against solid tumors of micelle-forming polymeric anticancer drug and its extremely long circulation in blood. Cancer Res 1991;51:3229–36.
20. Kataoka K, Harada A, Nagasaki Y. Block copolymer micelles for drug delivery: design, characterization and biological significance. Adv Drug Deliv Rev 2001;47: 113–31.
21. Matsumura Y, Hamaguchi T, Ura T, et al. Phase I clinical trial and pharmacokinetic evaluation of NK911, a micelle-encapsulated doxorubicin. Br J Cancer 2004;91: 1775–81.
22. Hamaguchi T, Matsumura Y, Suzuki M, et al. NK105, a paclitaxel-incorporating micellar nanoparticle formulation, can extend *in vivo* antitumour activity and reduce the neurotoxicity of paclitaxel. Br J Cancer 2005; 92:1240–6.
23. Uchino H, Matsumura Y, Negishi T, et al. Cisplatin-incorporating polymeric micelles (NC-6004) can reduce nephrotoxicity and neurotoxicity of cisplatin in rats. Br J Cancer 2005;93:678–87.
24. Folkman J. Anti-angiogenesis: new concept for therapy of solid tumors. Ann Surg 1972;175:409–16.
25. Gasparini G, Harris AL. Clinical importance of the determination of tumor angiogenesis in breast carcinoma: much more than a new prognostic tool. J Clin Oncol 1995;13:765–82.
26. Dickinson AJ, Fox SB, Persad RA, Hollyer J, Sibley GN, Harris AL. Quantification of angiogenesis as an independent predictor of prognosis in invasive bladder carcinomas. Br J Urol 1994;74:762–6.
27. Takahashi Y, Kitadai Y, Bucana CD, Cleary KR, Ellis LM. Expression of vascular endothelial growth factor and its receptor, KDR, correlates with vascularity, metastasis, and proliferation of human colon cancer. Cancer Res 1995;55:3964–8.
28. Williams JK, Carlson GW, Cohen C, Derose PB, Hunter S, Jurkiewicz MJ. Tumor angiogenesis as a prognostic factor in oral cavity tumors. Am J Surg 1994; 168:373–80.
29. Natsume T, Watanabe J, Koh Y, et al. Antitumor activity of TZT-1027 (Soblidotin) against vascular endothelial growth factor-secreting human lung cancer *in vivo*. Cancer Sci 2003;94:826–33.
30. Stacker SA, Caesar C, Baldwin ME, et al. VEGF-D promotes the metastatic spread of tumor cells via the lymphatics. Nat Med 2001;7:186–91.
31. Amoroso A, Del Porto F, Di Monaco C, Manfredini P, Afeltra A. Vascular endothelial growth factor: a key mediator of neoangiogenesis. A review. Eur Rev Med Pharmacol Sci 1997;1:17–25.
32. Cabral H, Nishiyama N, Okazaki S, Koyama H, Kataoka K. Preparation and biological properties of dichloro(1,2-diaminocyclohexane)platinum(II) (DACHPt)-loaded polymeric micelles. J Controlled Res 2005;101: 223–32.
33. Nishiyama N, Yokoyama M, Aoyagi T, Okano T, Sakurai Y, Kataoka K. Preparation and characterization of self-assembled polymer-metal complex micelle from *cis*-dichlorodiammineplatinum(II) and poly(ethylene glycol)-poly(α,β-aspartic acid) block copolymer in an aqueous medium. Langmuir 1999;15:377–83.
34. Kawato Y, Furuta T, Aonuma M, Yasuoka M, Yokokura T, Matsumoto K. Antitumor activity of a camptothecin derivative, CPT-11, against human tumor xenografts in nude mice. Cancer Chemother Pharmacol 1991;28:192–8.
35. Jain RK. Barriers to drug delivery in solid tumors. Sci Am 1994;271:58–65.
36. Zhang JA, Xuan T, Parmar M, et al. Development and characterization of a novel liposome-based formulation of SN-38. Int J Pharm 2004;270:93–107.
37. Lei S, Chien PY, Sheikh S, Zhang A, Ali S, Ahmad I. Enhanced therapeutic efficacy of a novel liposome-based formulation of SN-38 against human tumor models in SCID mice. Anticancer Drugs 2004;15:773–8.
38. Pal A, Khan S, Wang YF, et al. Preclinical safety, pharmacokinetics and antitumor efficacy profile of liposome-entrapped SN-38 formulation. Anticancer Res 2005;25:331–41.
39. Kraut EH, Fishman MN, LoRusso PM, et al. Final result of a phase I study of liposome encapsulated SN-38 (LE-SN38): safety, pharmacogenomics, pharmacokinetics, and tumor response [abstract 2017]. Proc Am Soc Clin Oncol 2005;23:139s.
40. Unezaki S, Maruyama K, Hosoda JI, et al. Direct measurement of the extravasation of polyethyleneglycol-coated liposomes into solid tumor tissue by *in vivo* fluorescence microscopy. Int J Pharmaceut 1996;144: 11–7.
41. Sasaki Y, Yoshida Y, Sudoh K, et al. Pharmacological correlation between total drug concentration and lactones of CPT-11 and SN-38 in patients treated with CPT-11. Jpn J Cancer Res 1995;86:111–6.
42. Onda T, Nakamura I, Seno C, et al. Superior antitumor activity of NK012, 7-ethyl-10-hydroxycamptothecin-incorporating micellar nanoparticle, to irinotecan [abstract 3062]. Proc Am Assoc Cancer Res 2006;47: 720s.

Available online at www.sciencedirect.com
SCIENCE DIRECT
Journal of Controlled Release 110 (2006) 514 – 521
journal of controlled release
www.elsevier.com/locate/jconrel

Induction of apoptosis in A549 human lung cancer cells by all-*trans* retinoic acid incorporated in DOTAP/cholesterol liposomes

Shigeru Kawakami, Sachiko Suzuki, Fumiyoshi Yamashita, Mitsuru Hashida *

Department of Drug Delivery Research, Graduate School of Pharmaceutical Sciences, Kyoto University, Sakyo-ku, Kyoto 606-8501, Japan

Received 20 July 2005; accepted 31 October 2005
Available online 19 December 2005

Abstract

All-*trans* retinoic acid (ATRA) has been shown to exert anti-cancer activities in a number of types of cancer cells. However, it has been reported that many NSCLC exhibited resistance to ATRA treatment. In the present study, we hypothesized that intracellular delivery of ATRA would overcome the ATRA resistance in A549 cells. Here, we investigated the induction of apoptosis by ATRA incorporated in cationic liposomes composed of DOTAP/cholesterol in A549 human lung cancer cells, which are insensitive (resistant) to the growth inhibitory effects of ATRA. The zeta potentials of DOTAP/cholesterol liposomes and DSPC/cholesterol liposomes were about +50 and −3 mV. In A549 cells, [^{3}H]ATRA incorporated in DOTAP liposomes showed increased cellular association compared with [^{3}H]ATRA or [^{3}H]ATRA incorporated in DSPC/cholesterol liposomes. ATRA incorporated in DOTAP/cholesterol liposomes showed much higher cytotoxic effects and apoptosis-inducing activity compared with ATRA or ATRA incorporated in DSPC/cholesterol liposomes. The enhanced expression of TIG3 mRNA tumor suppressor gene by ATRA incorporation into DOTAP/cholesterol liposomes might partly explain the mechanism of enhanced cytotoxicity and/or apoptosis. These observations provide valuable information to help in the design of differentiation therapy by ATRA in non-small cell lung carcinoma.

Keywords: Cationic liposomes; All-*trans* retinoic acid; Non-small cell lung carcinoma; Drug delivery system

1. Introduction

Differentiation therapy in oncology is defined as an approach to induce malignant reversion [1] that is based on the concept that cancer cells are normal cells that have been arrested at an immature or less differentiated state, lack the ability to control their own growth, and so multiply at an abnormally fast rate. Although differentiation therapy does not kill the cancer cells, it restrains their growth and allows the application of more conventional therapies (such as chemotherapy) to eradicate the malignant cells. Moreover, differentiation agents tend to be less toxic than conventional cancer treatment.

Several groups have demonstrated that all-*trans* retinoic acid (ATRA) can induce complete remission in a high proportion of acute promyelocytic leukemia patients [2,3]. ATRA has been shown to exert anti-cancer activities in a number of types of cancer cells [4–8]. The activity of ATRA is mediated by regulation of a variety of forms of gene expression through ATRA-dependent activation of retinoic acid receptors (RAR) and retinoid X receptors (RXR) on the nuclear membrane of cancer cells, leading to the growth inhibition, differentiation, and apoptosis of cancer cells [9]. Response of non-small cell lung carcinoma (NSCLC) to ATRA is modulated by additional factors. Recently, a novel retinoid-regulated gene, tazorotene-induced gene 3 (TIG3), also called retinoic acid receptor responder, has been cloned and characterized [10]. Since TIG3 has been identified as a potential tumor suppressor [10–12], TIG3 could be a biomarker for response to ATRA as well as a mediator of the antitumor effect of ATRA in NSCLC.

However, it has been reported that many NSCLC exhibit resistance to ATRA treatment [12–15]. In order to achieve successful cancer differentiation therapy against NSCLC, ATRA resistance needs to be overcome. One strategy to overcome ATRA resistance involves the development of an ATRA delivery carrier to the NSCLC. The lipophilicity of

Abbreviations: DOTAP, 1,2dioleoyl-3-trimethylammonium propane; DSPC, distearoylphosphatidylcholine.

* Corresponding author. Tel.: +81 75 753 4525; fax: +81 75 753 4575.
E-mail address: hashidam@pharm.kyoto-u.ac.jp (M. Hashida).

0168-3659/$ - see front matter © 2005 Elsevier B.V. All rights reserved.
doi:10.1016/j.jconrel.2005.10.030

ATRA is too high (logPCoct (the logarithmic *n*-octanol/water partition coefficient)=6.6) for efficient diffusion to the cellular membrane [16]; thus, it is quite likely that the cellular concentration for the action of ATRA is limited by its high lipophilicity. These observations prompted us to investigate whether the enhanced cellular uptake of ATRA by a drug carrier could be an efficient strategy to overcome ATRA resistance in NSCLC.

We have confirmed that most ATRA are incorporated in neutral liposomes due to their highly lipophilicity [17]. ATRA contain a carboxyl group; thus, ATRA would be more stably incorporated in cationic liposomes. Cationic liposomes are selectively accumulated in angiogenic endothelial cells in tumors [18] and remain largely confined to the tumor site compared with anionic or neutral liposomes after intravenous injection [19]. We have demonstrated that 50% of cationic liposomes composed of DOTAP/cholesterol accumulate in the lung 1 min after intravenous injection [20]. Cationic liposomes are internalized by endocytosis in these cells. Taking these findings into consideration, DOTAP/cholesterol liposomes are expected to be an effective drug carrier of ATRA for intracellular-NSCLC-selective delivery to overcome ATRA resistance in NSCLC.

In the present study, we investigated the induction of apoptosis by ATRA incorporated in DOTAP/cholesterol liposomes in A549 human lung cancer cells, which are insensitive (resistant) to the growth inhibitory effects of ATRA [12,14,15]. After application of ATRA incorporated in DOTAP/cholesterol liposomes in A549 cells, the cellular uptake mechanism, cytotoxicity, induction of apoptosis, and TIG3 mRNA expression were evaluated. Results were compared with free ATRA or ATRA incorporated in neutral liposomes (DSPC/cholesterol liposomes).

2. Materials and methods

2.1. Materials

DOTAP, DSPC, were obtained from Avanti Polar Lipids, Inc. (Alabaster, AL, USA) and Sigma-Aldrich Co. (St. Louis, MO, USA). Chol and Clear-Sol I were obtained from Nacalai Tesque, Inc. (Kyoto, Japan), and Soluene 350 was purchased from Packard Co., Inc. (Groningen, The Netherlands). Dulbecco's modified Eagle's minimum essential medium (DMEM) and fetal bovine serum (FBS) was obtained from Nissui Pharmaceutical Co., Ltd. (Tokyo, Japan) and Biowhittaker (Walkersville, MD, USA). ATRA and [^{3}H]ATRA was purchased from Wako Pure Chemicals Industry, Ltd. (Osaka, Japan) and NEN Life Science Products, Inc. (Boston, USA). MagExtractor-RNA kit was obtained from Toyobo Co., Ltd. (Osaka, Japan). SYBR-Green I was purchased from Takara Bio, Inc. (Shiga, Japan). All other chemicals were of the highest purity available.

2.2. Cell line

A549 cells were routinely grown in DMEM medium supplemented with 10% FBS, 100 IU/ml penicillin, 100 μg/ml streptomycin, and 2 mM L-glutamine (all from Invitrogen Co., Carlsbad, CA, USA) in 5% CO_2, humidified air at 37 °C.

2.3. Preparation of liposomes

Liposomes were prepared by the method described previously [21,22]. Briefly, DOTAP, DSPC and cholesterol were used to prepare the liposomes. The liposomes, DOTAP/cholesterol (1:1, molar ratio) and DSPC/cholesterol (3:2, molar ratio), were prepared with or without ATRA. ATRA was mixed at the molar ratio of 1:100 of the total lipid content of the liposomes. In the cellular association experiments, liposomes were labeled with a tracer amount of [^{3}H]ATRA. Briefly, the mixture, with or without [^{3}H]ATRA, was first dissolved in chloroform. After vacuum drying and desiccation, pH 7.4 phosphate-buffered saline (−) (PBS (−)) was added for hydration. The preparation was sonicated and passed through a 0.45-μm filter for sterilization.

2.4. Characterization of liposomes

The lipid content of the liposomes was determined by a cholesterol E-test Wako kit (Wako Pure Chemicals Industry, Ltd., Osaka, Japan). The liposomal loading of ATRA was estimated by absorbance at 340 nm after dissolving ATRA incorporated in liposomes in ethanol since the ATRA alone is soluble in ethanol. The zeta potentials of liposomes were measured in 150 mM sodium chloride (NaCl) (pH 7.0) with a laser electrophoresis zeta potential analyzer (LEZA-700, Otsuka Electronics Co., Ltd., Osaka, Japan). The particle sizes of the liposomes were measured in 150 mM NaCl using dynamic light scattering (DLS-7000, Otsuka Electronics Co., Ltd., Osaka, Japan).

2.5. Evaluation of ATRA incorporated in liposomes

The methods used to determine the incorporation ratio of ATRA in liposomes were as described for the liposomal studies [23,24]. Briefly, the [^{3}H]ATRA-incorporated liposomes were ultrafiltered using a micropartition system (Sartorion VIVASPIN 2 ml concentrator 5000 MWCO PES; Vivascience AG, Hannover, Germany) at 1500×*g* for 15 min. The concentration based on the radioactivity in the preparation (C_T) and in the ultrafiltrate (C_W) was assayed by scintillation counting. The equation for the incorporation ratio in the liposomes was as follows:

$$\text{Incorporation ratio } (\%) = ((C_T - C_W)/C_T) \times 100.$$

2.6. Cellular association study

The cellular association study was performed by the method described previously [25,26]. The A549 cells were plated on a 12-well cluster dish at a density of 5×10^4 cells/3.8 cm^2. Twenty-four hours later, the cells were washed with 1.0 ml PBS (−) and incubated with 1.0 ml medium containing